Dalton Transactions

ROYAL SOCIETY OF CHEMISTRY

PAPER

View Article Online
View Journal | View Issue

Cite this: *Dalton Trans.*, 2024, **53**, 8692

Molecular two-point recognition of fructosyl valine and fructosyl glycyl histidine in water by fluorescent Zn(II)-terpyridine complexes bearing boronic acids†

María K. Salomón-Flores, [a] Josue Valdes-García, [a] Alejandro O. Viviano-Posadas, [a] Diego Martínez-Otero, [a,b] Joaquín Barroso-Flores, [a,b] Iván J. Bazany-Rodríguez [a] and Alejandro Dorazco-González *[a]

Selective recognition of fructosyl amino acids in water by arylboronic acid-based receptors is a central field of modern supramolecular chemistry that impacts biological and medicinal chemistry. Fructosyl valine (FV) and fructosyl glycyl histidine (FGH) occur as N-terminal moieties of human glycated hemoglobin; therefore, the molecular design of biomimetic receptors is an attractive, but very challenging goal. Herein, we report three novel cationic Zn-terpyridine complexes bearing a fluorescent *N*-quinolinium nucleus covalently linked to three different isomers of strongly acidified phenylboronic acids (*ortho*-, **2Zn**; *meta*-, **3Zn** and *para*-, **4Zn**) for the optical recognition of FV, FGH and comparative analytes (D-fructose, Gly, Val and His) in pure water at physiological pH. The complexes were designed to act as fluorescent receptors using a cooperative action of boric acid and a metal chelate. Complex **3Zn** was found to display the most acidic $-B(OH)_2$ group (pK_a = 6.98) and exceptionally tight affinity for FV (K = 1.43 × 10^5 M^{-1}) with a strong quenching analytical response in the micromolar concentration range. The addition of fructose and the other amino acids only induced moderate optical changes. On the basis of several spectroscopic tools (^1H, ^{11}B NMR, UV-Vis, and fluorescence titrations), ESI mass spectrometry, X-ray crystal structure, and DFT calculations, the interaction mode between **3Zn** and FV is proposed in a 1 : 1 model through a cooperative two-point recognition involving a sp^3 boronate–diol esterification with simultaneous coordination bonding of the carboxylate group of Val to the Zn atom. Fluorescence quenching is attributed to a static complexation photoinduced electron transfer mechanism as evidenced by lifetime experiments. The addition of FGH to **3Zn** notably enhanced its emission intensity with micromolar affinity, but with a lower apparent binding constant than that observed for FV. FGH interacts with **3Zn** through boronate–diol complexation and coordination of the imidazole ring of His. DFT-optimized structures of complexes **3Zn**–FV and **3Zn**–FGH show a picture of binding which shows that the Zn-complex has a suitable (B···Zn) distance to the two-point recognition with these analytes. Molecular recognition of fructosyl amino acids by transition-metal-based receptors has not been explored until now.

Received 28th January 2024,
Accepted 23rd April 2024

DOI: 10.1039/d4dt00260a

rsc.li/dalton

Introduction

The development of selective boronic acid-based receptors for glyco-amino acids related to glycated hemoglobin (HbA1c) such as fructosyl L-valine (FV) and fructosyl-valyl-histidine (FVH) remains a challenge in modern supramolecular chemistry and analytical sciences due to their potential application in sensing, separation, development of new concepts of glycopeptides recognition,[1–5] as well as the diagnosis of sugar-related diseases and medicinal chemistry.[6,7]

FV occurs as an N-terminal unit of human HbA1c inside β-subunits (fructosyl-Val-His-Leu-Thr...)[8,9] and typically serves

[a]*Institute of Chemistry, National Autonomous University of Mexico, Ciudad Universitaria, 04510 CDMX, Mexico. E-mail: adg@unam.mx*
[b]*Centro Conjunto de Investigación en Química Sustentable, UAEM-UNAM, Carretera Toluca-Atlacomulco Km 14.5, C. P. 50200, Toluca, Estado de México, Mexico*

†Electronic supplementary information (ESI) available: General information, X-ray crystallographic data, ^1H, ^{13}C, ^{11}B NMR spectra for all compounds and UV-Vis and fluorescence titration experiments. CCDC 2279289 and 2279290. For ESI and crystallographic data in CIF or other electronic format see DOI: https://doi.org/10.1039/d4dt00260a

as a target test molecular moiety and chemical model to mimic the diagnosis of type 2 diabetes mellitus.[1,10,11] To date, an overwhelming majority of FV and related fructosyl amino acid detection methods are based on chromatography separation-mass spectrometry,[10,12] mutant proteins,[13] electrochemical biosensors,[2,9,14–18] and Pt/Au-amperometric nanomaterials[5,9,19,20] that contain the fructosyl amino-acid oxidase. These enzymatic assay systems still suffer from some drawbacks such as multiple steps for their construction, long analysis times and the requirement for specialized labs. Additionally, FV sensing can be achieved by non-enzymatic systems using boronic acid-appended redox active species such as Au/C-electrodes functionalized with thiophene-boronic acid,[21] ferrocenylboronic acid,[22,23] and vinylphenylboronate-polymers[24] where the FV recognition is driven by the formation of an sp^3-boronated ester with a sugar moiety. It is well known that simple phenylboronic acid (PBA) has a higher affinity for catechol fragments, open-chain polyols and anionic species than for fructose in water (binding constant K = 160 M^{-1});[25] therefore, these boronic acid-based materials are not particularly selective and interference from biogenic catecholamines, phosphorylated anions, dicarboxylates, and sorbitol/mannitol can be a problem.[26–31] Furthermore, this affinity of PBA towards fructose is suitable to recognize/sense FV in the millimolar concentration range, but not lower, which is highly desired for its intended applications.

While the need for selective optical receptors for FV and FVH is evident, to the best of our knowledge, fluorescent molecular receptors for their quantification have not yet been developed.

Among different saccharide recognition techniques, fluorescence is particularly desired due to its known high sensitivity, quick and direct analytical response.[32]

Arylboronic acids can form reversible covalent bonds with 1,2-diols in basic aqueous media[33] where the binding strength of boronic acid–1,2-diol ester depends on the orientation of the analyte's vicinal hydroxyl groups,[34] the acidity of the boronic acid,[35] and the influence of substituent groups to stabilize the sp^3-boronate ester.[28] In the last few decades, phenylboronic acid fluorophores have been demonstrated to be an outstanding tool for recognizing and sensing monosaccharides,[36] catechol-based neurotransmitters,[37] nucleotides,[38] sialic acid,[39] glucosamine,[40] ginsenosides,[41] glycated hemoglobin,[42] and in general, 1,2-dihydroxy-substituted derivatives.[33,43] However, the recognition of fructosyl amino acids (Amadori products)[44] remains largely unexplored. In principle, it should be possible to have a selective optical chemosensor for FV by using a fluorescent receptor with multiple and high-affinity binding sites for FV or target derivatives.

On the other hand, reports in the context of coordination chemistry have shown that Zn(II)-terpyridine complexes are effective binding motifs for carboxylate anions and imidazole fragments[45] *via* direct coordination due to their versatile coordination number and strong Lewis acidity of the Zn atom.[46,47] There is only one report in the literature showing that FV and some Amadori products, such as fructosyl-glycine (FG), can bind divalent transition metal ions (*e.g.* Cu(II), Ni(II)) with an affinity of about 10^3 M^{-1} in water.[44]

In this study, we have designed and prepared three novel cationic luminescent Zn-terpyridine complex-based receptors bearing a strongly acidified phenylboronic acid to bind through cooperative two sites to FV or fructosyl-Gly-His (FGH) which is a chemical model of the sequence fructosyl-Val-His from HbA1c with the same terminal residues.[9] FV is the most common chemical model of HbA1c used in detection/recognition studies and clinical diagnostics.[2] However, there is recent interest in cooperatively recognizing fructose and histidine residues to improve the specificity of sensors.[5,48] In this work, for the first time, we explored developing a fluorescent receptor functional for FV and FGH through cooperative two-point recognition that includes a coordination bond and a covalent boronate–diol bond.

The baseline expectation for these Zn-receptors is that phenylboronic acid can form stable complexes with the fructosyl motif and the Zn(II) atom can interact with the carboxylate group from valine (FV) or the imidazole ring from histidine (FGH). The results obtained for a series of fluorescent Zn-terpyridine-4′-quinolinium complexes bearing three different isomers of boronic acids, including synthesis, crystal structures, acid–base properties, spectroscopic recognition and theoretical DFT calculations are summarized below.

Results and discussion

Synthesis and crystal structure

For these investigations, three isomers **2Zn**, **3Zn** and **4Zn** involving two Lewis acids of different nature (B and Zn atoms) as binding sites for fructosyl-amino acids were successfully prepared by the three-step path described in Scheme 1. The synthesis was initiated with the preparation of a terpyridine bearing a quinoline moiety at position 4′ of the central pyridine ring by the Kröhnke reaction to give **1**, and subsequent treatment with the corresponding isomer of (bromo-methyl) phenylboronic acid in dry CH_3CN under a N_2 atmosphere to afford the cationic ligands (L), **2–4.** These ligands were characterized by ^1H and ^{13}C NMR spectroscopy, ESI-MS (+) and ATR-IR. The expected number of NMR signals and MS peak of these ligands were consistent with their structures (Fig. S1–S15†). For comparative purposes, ligand **5**, which lacks boronic acid, was synthesized *via* the same synthetic route and characterized (Fig. S16–S19†), using benzyl bromide instead of a (bromo-methyl)phenylboronic acid. The Zn-complexes were obtained upon direct complexation with 1.1 equiv. of $ZnBr_2{\cdot}2H_2O$ in CH_3CN–EtOH at r.t. In all cases, the bromide salts of Zn-complexes were obtained as pink pale crystalline powders and were pure according to ^1H, ^{11}B, and ^{13}C NMR spectroscopy (Fig. S20–S37†), ESI-MS and elemental analysis (C, H, N). One charged state for the three isomers **2Zn**, **3Zn** and **4Zn**, monoanionic species at m/z = 880.81, corresponding to $\{[ZnL]^{3+} + 4Br^-\}^-$, was clearly observed and isotopically

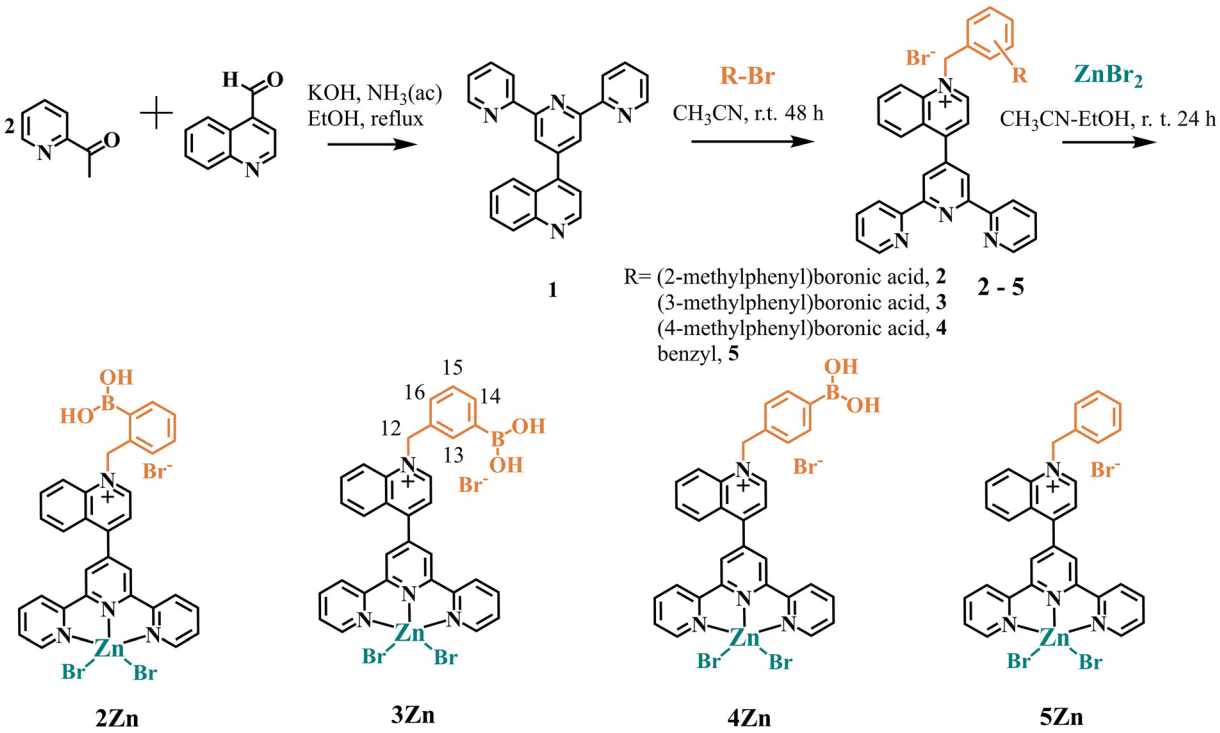

Scheme 1 Synthesis of Zn(II)-complexes-based fluorescent receptor used in this work.

resolved from their respective analysis by a negative scan of ESI (Fig. S23, S29 and S33†).

The ^{11}B NMR spectra of the three isomeric Zn-complexes in CD_3OD–DMSO-d_6 displayed only one signal at ~27 ppm (Fig. S22, S27 and S32†). This value corresponds to the sp^2-hybridized trigonal boron atom, however, this signal is upfield shifted compared to simple neutral PBA (δ = 30 ppm).[49] As we have recently shown, this upfield shift of the signal in ^{11}B NMR can be the result of the strong acidification of the phenylboronic groups by the delocalized positive charge on the quinolinium ring.[50] Along this line, Lakowicz has previously reported strong acidification of phenylboronic acids when covalently linked to 6-methoxyquinolinium nuclei.[51]

X-ray crystal structures were obtained for the hydrated bromide salts of **3Zn** and **5Zn**. Fig. 1 shows a perspective view of these molecules. Tables S1–S3† contain the crystallographic data and parameters of hydrogen bonds within the crystal packing of these complexes.

X-ray structural analysis of **3Zn** confirms the presence of sp^2-hybridized boronic acid and a trigonal planar geometry ($\sum\measuredangle(X\text{–}B\text{–}X)$ = 359.99°) which is consistent with its ^{11}B NMR spectrum in solution. The angle between the –$B(OH)_2$ plane and the phenyl ring is 46.55°. The –$B(OH)_2$ group is stabilized by a Br^- anion and a water molecule through hydrogen bonds (the parameters of hydrogen bonds are compiled in Table S2†). The structural analysis showed that the Zn(II) atoms in **3Zn** and **5Zn** have a distorted square-pyramidal geometry with a [ZnN_3Br_2] coordination sphere. For both crystals, the rings of central pyridine (terpy) and quinoline are significantly out of coplanarity. The angles are 63.25° and 58.42° for **3Zn** and **5Zn**, respectively. The distortion in the coplanarity between these rings seems to be primarily an electronic rather than steric effect.[52]

A review of the crystal packings of **3Zn** and **5Zn** reveals the presence of strong π···π stacking interactions between central and external pyridine rings (Fig. 2).

Optical and acid–base properties

The bromide salts of cationic complexes **2Zn**, **3Zn**, **4Zn** and **5Zn** are soluble in buffered water at pH = 7.4 (10 mM MOPS) and follow very well the Lambert–Beer law up to 100 μM by fluorescence spectroscopy; thus, these conditions were used for further spectroscopic studies. The absorption and fluorescence maxima of all Zn-complexes at physiological pH are compiled in Table 1. The blue emission at ~450 nm in these quinolinium-based compounds is typically attributed to intramolecular charge transfers (ICTs) in the excited state.[53]

The acid–base properties of Zn-complexes were explored by fluorimetric pH-titration experiments. Fig. 3A shows the family of fluorescence spectra of **3Zn** at different pH values and its inset illustrates the fitting of the profile at a single wavelength *vs.* pH to the theoretical equation (see Fig. S46† for fluorescence spectra–pH of **2Zn** and **4Zn**).

The pH-profiles of fluorescence intensity at 450 nm for the three isomers and their pK_a values are shown in Fig. 3B and Table 2. The pK_a values estimated for the –$B(OH)_2$ group in **2Zn** and **3Zn** are close to 7.0. This finding is relevant to our objectives because it reveals that the boronic acid groups are

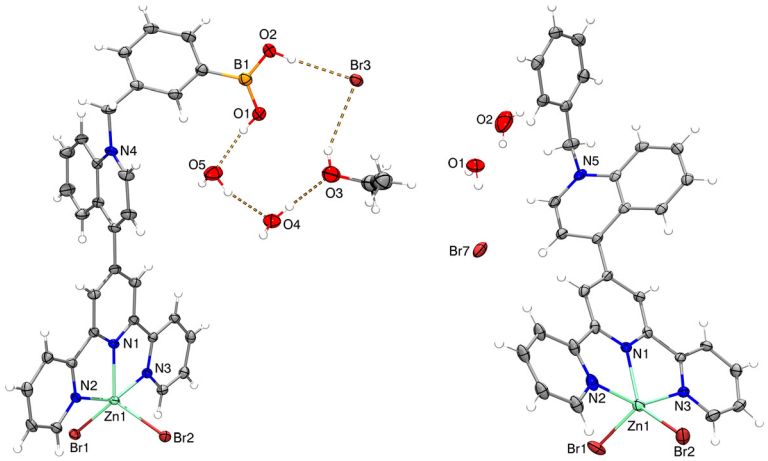

3Zn 5Zn

Fig. 1 ORTEP diagrams at 50% of probability for bromide salts of **3Zn** and **5Zn**. B–O–H···Br$^-$, B–O–H···O and O–H···O hydrogen bonds for **3Zn** are shown as dashed lines. For complex **5Zn**, three independent molecules were observed in the unit cell (only one of which is shown). Additional solvent molecules and the tetrabromozincate counterion were omitted for clarity.

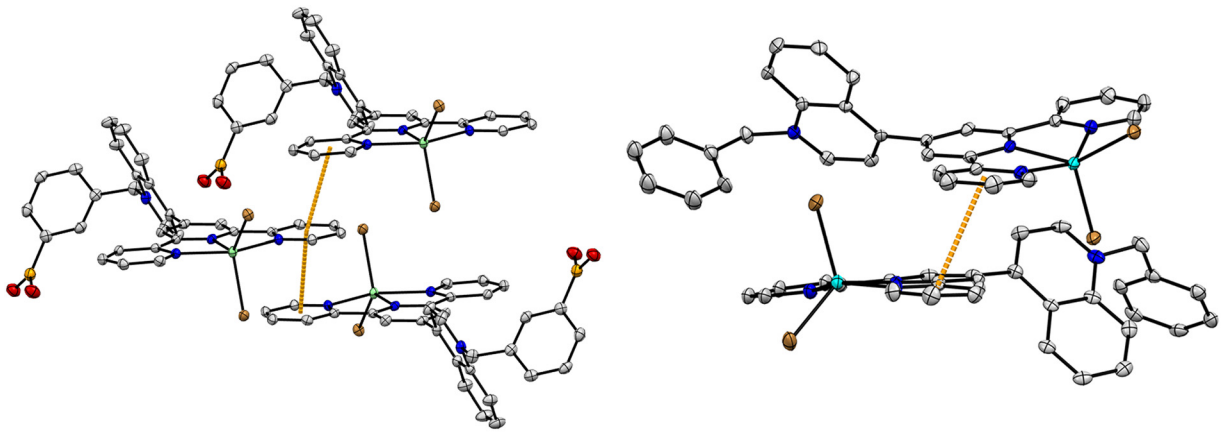

3Zn 5Zn

Fig. 2 Crystal packing diagrams of complexes **3Zn** and **5Zn**. The intermolecular π···π distances (3.547(5)–3.608(6) Å, orange dashed lines) for **3Zn** and (3.592(4) Å) for **5Zn** were measured between the centroids of the aromatic rings.

Table 1 Absorption and emission (λ_{ex} = 330 nm) maxima (nm) of Zn-complexes in water at pH = 7.40 and pK_a values estimated from fluorimetric titration experiments

Complex	λ_{abs} (log ε)	λ_{em}	Fluorimetric titration, pK_a
2Zn	278 (4.21); 285 (4.24); 330 (4.19)	446	7.09 ± 0.02
3Zn	279 (4.14); 286 (4.20); 329 (4.08)	450	6.98 ± 0.03
4Zn	278 (4.13); 285 (4.09); 329 (4.02)	445	7.40 ± 0.04

in their sp^3 anionic sugar bond form at pH = 7.40, enabling the fructosyl recognition under "physiological" conditions.

The calculated pK_a values for **2Zn** (pK_a = 7.09) and **3Zn** (pK_a = 6.98) are lower than those reported for free phenylboronic acid (pK_a = 8.8)[25] and for typical boronic acid-based receptors for fructose that contain viologen or fluorene motifs.[34,49,54] This fact is not unexpected because it is well known that the cationic nature of the quinolinium ring covalently appended to boronic acid reduces the pK_a values up to two orders of magnitude.[32,51,55]

On the other hand, very low pK_a values ranging from 6.70 to 7.90 have been reported previously for quinolinium[51,55] and isoquinolinium[50] nuclei-bearing isomers (*ortho*, *meta*) of phenylboronic acids. These values are consistent with those estimated for **2Zn** and **3Zn**.

Table 2 compiles the pK_a results obtained from fluorescence spectroscopy of **2Zn**, **3Zn** and **4Zn** and for comparison, lists pK_a values found in the literature for related compounds containing a boronic acid-substituted benzyl pyridinium or benzyl quinolinium motif (see Fig. 4).

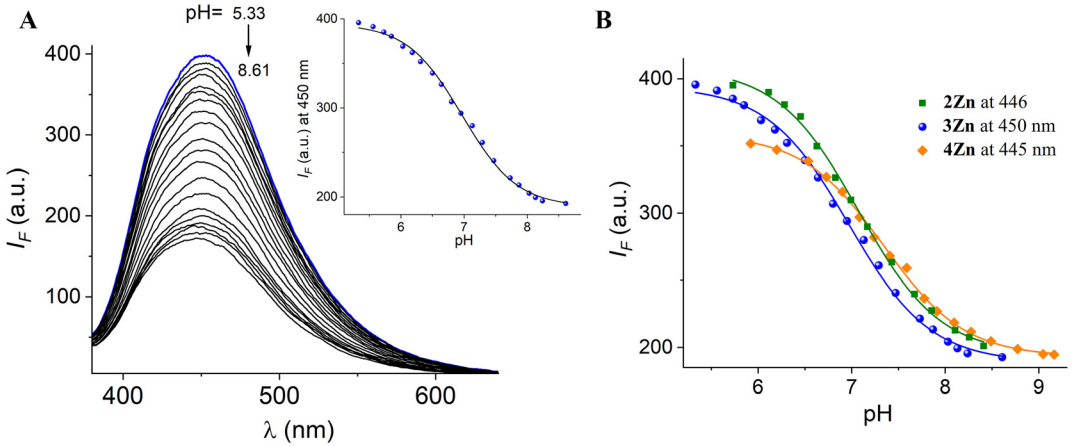

Fig. 3 (A) Fluorescence spectra of **3Zn** (20 μM) in buffered aqueous solution (λ_{ex} = 330 nm) at different pH values. (B) The observed pH-titration profiles at the emission maximum of each Zn-complex.

Table 2 Comparison of pK_a values for **2Zn**, **3Zn** and **4Zn** determined *via* fluorescence with literature values reported for structurally similar (Fig. 4) derivatives **6–8**

		Literature values		
Complex	pK_a fluorescence	Ref. 49	Ref. 51	Ref. 55
2Zn	7.09	8.80 (**6**-*ortho*)	7.90 (7-*ortho*)	6.70 (**8**-*ortho*)
3Zn	6.98	7.80 (**6**-*meta*)	7.70 (7-*meta*)	7.55 (**8**-*meta*)
4Zn	7.40	8.10 (**6**-*para*)	7.90 (7-*para*)	7.80 (**8**-*para*)

An inspection of these data indicates that, in general, the pK_a values of the *meta* and *ortho* isomers tend to be lower, between 0.2 and 1.1 units, as compared to the *para* isomer. This trend is also observed in our Zn-complexes.

Typically, this effect is ascribed to the fact that the quaternary nitrogen of the quinolinium moiety not only reduces the pK_a of the boronic acids by an electron-withdrawing inductive effect, but also electrostatically stabilizes the sp^3-boronate anion formed.[49,51,55] Therefore, the pK_a value of the *para* isomer is expected to be higher due to the greater distance between the $-B(OH)_2$ group and the quinolinium ring compared to *ortho* or *meta* isomers, as observed in the value of **4Zn** and with a different set of isomers in Table 2.

It is noteworthy that if the pK_a were driven simply by interaction-induced stabilization and the distance between the quinolinium and the sp^3-boronate anion formed as commonly described, one would expect the *ortho* isomer to always be the more acidic species; however, the data in Table 2 for **6** and **7** and the values of our complexes show that the *meta* isomer is slightly more acidic. Therefore, other side effects that stabilize the boronate anion cannot be ruled out as a steric effect which can be considerable, particularly for the *ortho* isomer.

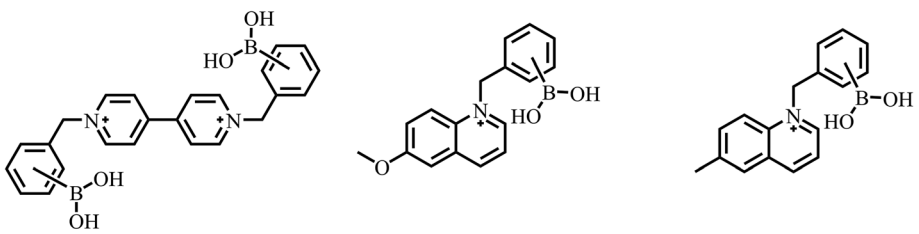

Fig. 4 Structure of compounds **6**,[49] **7**[51] and **8**[55] containing a boronic acid-substituted benzyl pyridinium or quinolinium fragment for which pK_a values have been previously reported (Table 2).

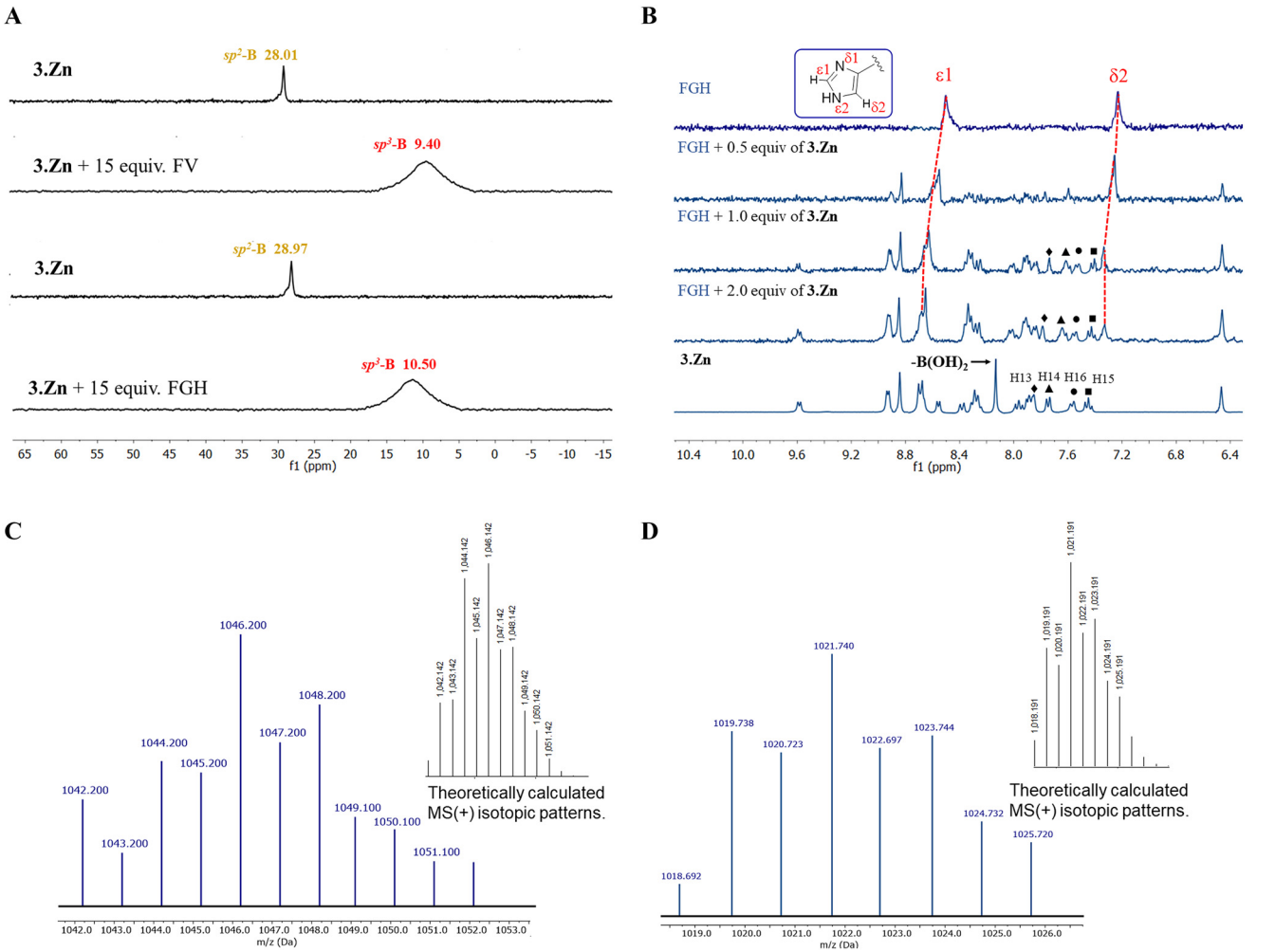

Fig. 5 (A) ^{11}B NMR spectra (96 MHz, 25 °C) of **3Zn** (2.0 mM) in the absence and presence of 15.0 equiv. of FV or FGH in CD_3OD–DMSO-d_6 (4 : 1, v/v). (B) Partial ^{1}H NMR (300 MHz, 25 °C) spectra of free FGH (3.0 mM) + **3Zn** (0, 0.5, 1.0, and 2.0 equiv.) and spectrum of free **3Zn** (3.0 mM) in D_2O–DMSO-d_6 (8 : 2, v/v). Positive scan ESI-MS spectrum in H_2O–CH_3OH (1 : 1, v/v) solution containing **3Zn** + 3.0 equiv. of FV (C) and H_2O–EtOH (1 : 1, v/v) of **3Zn** + FGH (D). Inset: calculated isotopic distribution for monocationic 1 : 1 supramolecular complexes.

Fructosyl amino acid binding studies

Taking advantage of the fact that the **3Zn** complex possesses the most acidic –$B(OH)_2$ group (pK_a = 6.98), this compound was studied as a model receptor for FV and FGH by different spectroscopic experiments. The first evidence for the high affinity of **3Zn** for these two fructosyl amino acids was obtained by ^{11}B and ^{1}H NMR measurements. Fig. 5A illustrates the experiments of **3Zn** with FV and FGH monitored by ^{11}B NMR spectroscopy. Upon the addition of 15 equiv. of FV to a solution of **3Zn** (2.0 mM) the initial signal for the sp^2-B atom at 28.01 ppm disappeared and a new broadened signal at 9.40 ppm arose for the sp^3-B atom. A similar ^{11}B NMR response was observed with FGH. This chemical shift ($\Delta\delta$ = 18.61 ppm for FV and 18.47 ppm for FGH) of the ^{11}B NMR signals is characteristic of the formation of an sp^3-boronate complex with sugars.[49,56] Thus, the shift in ^{11}B NMR signals from sp^2-B to sp^3-B confirms the binding of the fructosyl moieties for both analytes to the **3Zn** complex through the formation of a boronate ester.

Particularly, for the case of FGH, we investigated the potential coordination of the imidazole ring of His with the Zn(II) center by a ^{1}H NMR titration experiment in D_2O–DMSO-d_6. The addition of **3Zn** (0–2.0 equiv.) to the solution of FGH (3.0 mM) induces a notable downfield shift ($\Delta\delta$ = 0.31 ppm) of the ε1-proton corresponding to the imidazole ring as is shown in Fig. 5B. The downfield shift can be assigned to the effective coordination of the imidazole ring to the Zn(II) center. This metal binding to the heterocycle is not unexpected because the Nε2-atom of imidazole is undoubtedly the strongest bonding donor atom due to its high basicity and a favorable electrostatic potential as is evidenced by the great occurrence of this coordination bond (Zn–Nε2) in Zn-histidine complexes and Zn-proteins by NMR spectroscopic studies.[57]

Furthermore, a comparison between the ^{1}H NMR spectra of free **3Zn** and FGH + **3Zn** shows that only the aromatic H13–16

protons of the phenylboronic acid ring (see Scheme 1 for numbering of the structure) are affected. Reversible esterification of boronic acid with the fructosyl fragment induces an upfield shift of ~0.22 ppm for the aromatic H13–16 protons with a simultaneous disappearance of the signal of $-B(OH)_2$ at 8.12 ppm; practically, the rest of the protons of **3Zn** are not affected.

Mass spectrometry has been used in the past to study boronate–diol complexes.[32] The mass spectra of **3Zn** in the presence of 3.0 equiv. of FV or FGH obtained by a positive scan of ESI in aqueous media showed practically one charged species at m/z = 1046.2 and 1021.7, respectively (Fig. 5C and D).

These peaks were isotopically resolved and match very well the theoretical distribution for the monocationic complexes $\{[\mathbf{3Zn}] + 2(Br)^- + FV + 2(CH_3OH) + H_2O\}^+$ (calc. $C_{44}H_{51}BBr_2N_5O_{10}Zn$, m/z 1046.14) and $\{[\mathbf{3Zn}] + Br^- + FGH + 1(EtOH)\}^+$ (calc. $C_{47}H_{47}BBrN_8O_9Zn$, m/z = 1021.20) corresponding to 1 : 1 supramolecular complexes **3Zn**–FV and **3Zn**–FGH, respectively. [**3Zn**] species corresponds to the tricationic Zn-complex without bromide ions. In both cases, boronate/carboxylate groups balance the charges.

Fluorescent chemosensing studies of fructosyl amino acids

Addition of FV, FGH, Fru, His, Gly and Val in a micromolar concentration range to aqueous solutions of **2Zn**, **3Zn** and **4Zn** at pH = 7.4 induced small changes, but changes in the UV-Vis spectra of Zn-complexes with FV and FGH were clearly observed. As an example, Fig. S47† shows the titration experiment for **3Zn** with increasing concentrations of FV (0–180 μM), from which the apparent binding constant, $K = (1.36 \pm 0.12) \times 10^5$ M^{-1}, can be well calculated by fitting to a 1 : 1 model (see inset, Fig. S47†). Three isosbestic points at 290, 310 and 344 nm were observed, which indicates that only two species are in equilibrium (free complex **3Zn** and its complexed form with FV).

To obtain a more sensitive optical response, we tested the affinity/sensing of **3Zn** towards FV, FGH and comparative analytes (Fru, Val, Gly and His) by steady-state fluorescence spectroscopy in pure water.

Initially, the relative fluorescence selectivity was analyzed. FV, FGH, Fru, Val, Gly, and His ($[\text{analyte}]_{\text{final}}$ = 100 μM) were added to an aqueous solution (10 mM MOPS, pH = 7.4) of **3Zn** (20 μM) and the emission spectra (λ_{ex} = 330) was recorded (Fig. 6A). In addition, Fig. 6B shows the emission intensity change at 450 nm of **2Zn** and **3Zn** upon the addition of these analytes. Overall, Fru, Val and Gly gave a low quenching response I_F < 7% of its starting emission I_0. The addition of FV notably decreases the emission intensity by *ca.* ~29% and 52% for **2Zn** and **3Zn**, respectively. This quenching effect is not unexpected because the boronic acid fluorophores or Zn-complexes typically show a complexation-induced quenching analytical response as a result of a photoelectron transfer (PET) mechanism when forming a boronate–diol ester[36,58] or by the coordination of carboxylates to the Zn atom.[59]

In contrast, the addition of His induced a slight enhancement in intensity (~10%) for both Zn-complexes. Optical recognition of His by Zn-terpy complexes with the turn-on signal has been previously reported[60] and the fluorescence enhancement was attributed to (1) the increase in the rigidity of the system by effective coordination of the imidazole ring of His and (2) the disappearance of any intramolecular charge transfer processes in the receptor-anion complex.[60] Furthermore, the coordination of His decreases the degree of hydration of the complex which should favor emission.[47]

The addition of FGH to the buffered solution of **3Zn** generated a strong enhancement fluorescence of approximately 90% with a bathochromic effect ($\Delta\lambda$ = 12 nm) in the emission maxima (Fig. 6B). A similar effect was observed for **2Zn** but with a smaller intensity improvement (53%) than that observed for **3Zn**.

The strong fluorescence change induced by FV and FGH suggests that fructosyl amino acids have greater affinity than their chemical constituents (Fru or amino acids) separately which can be explained by a two-point cooperative recognition which does not seem feasible for Fru or amino acids. To verify this selectivity, we determined the binding constants for all analytes through fluorimetric titration experiments. Fig. 7 shows the fluorimetric titrations of the most acidic complex, **3Zn** with FV and FGH.

In general, the profile curves (shown in the insets) can be well fitted to a 1 : 1 binding model with non-linear least-squares treatment using eqn (1) to obtain apparent binding constants $K_{\mathbf{3Zn}-FV} = (1.43 \pm 0.10) \times 10^5$ and $K_{\mathbf{3Zn}-FGH} = (1.02 \pm 0.07) \times 10^5$, where I_F is the observed intensity, I_0 is the intensity of free **3Zn** (R), ΔI_∞ is the change induced by the analyte at saturation, $[A]_T$ is the total concentration of the guest and K is the apparent binding constant.

$$I_F = I_0 + \frac{\Delta I_\infty \left\{ [R]_T + [A]_T + \frac{1}{K} - \left[\left([R]_T + [A]_T + \frac{1}{K} \right)^2 - [4][R]_T[A]_T \right]^{0.5} \right\}}{2[R]_T} \quad (1)$$

The apparent complexation constant determined from fluorescence matches well with the value estimated by the UV-Vis titration (*vide supra*), indicating that the interaction occurs mainly in the ground state.

The fitted fluorimetric curves to the 1 : 1 model for all analytes with **2Zn** and **3Zn** are shown in Fig. 8A and B (see Fig. S48† for **4Zn**). The estimated apparent binding constants (error < 10%) are compiled in Table 3.

A detailed inspection of the results in Table 3 shows that, indeed, tendencies in affinity constants are similar for the most acidic and effective receptors (**3Zn** and **2Zn**). For example, **3Zn** binds FV two or three orders of magnitude tighter than it binds Fru or Val ($<10^3$ M^{-1}) and **3Zn** binds FGH two orders of magnitude larger than Fru or His ($\sim 10^3$ M^{-1}).

One can deduce that the combination of the metal coordination with boronate–diol in the *meta* isomer of phenylboronic acid leads to substantial increases in the complexation between **3Zn** and FV or FGH.

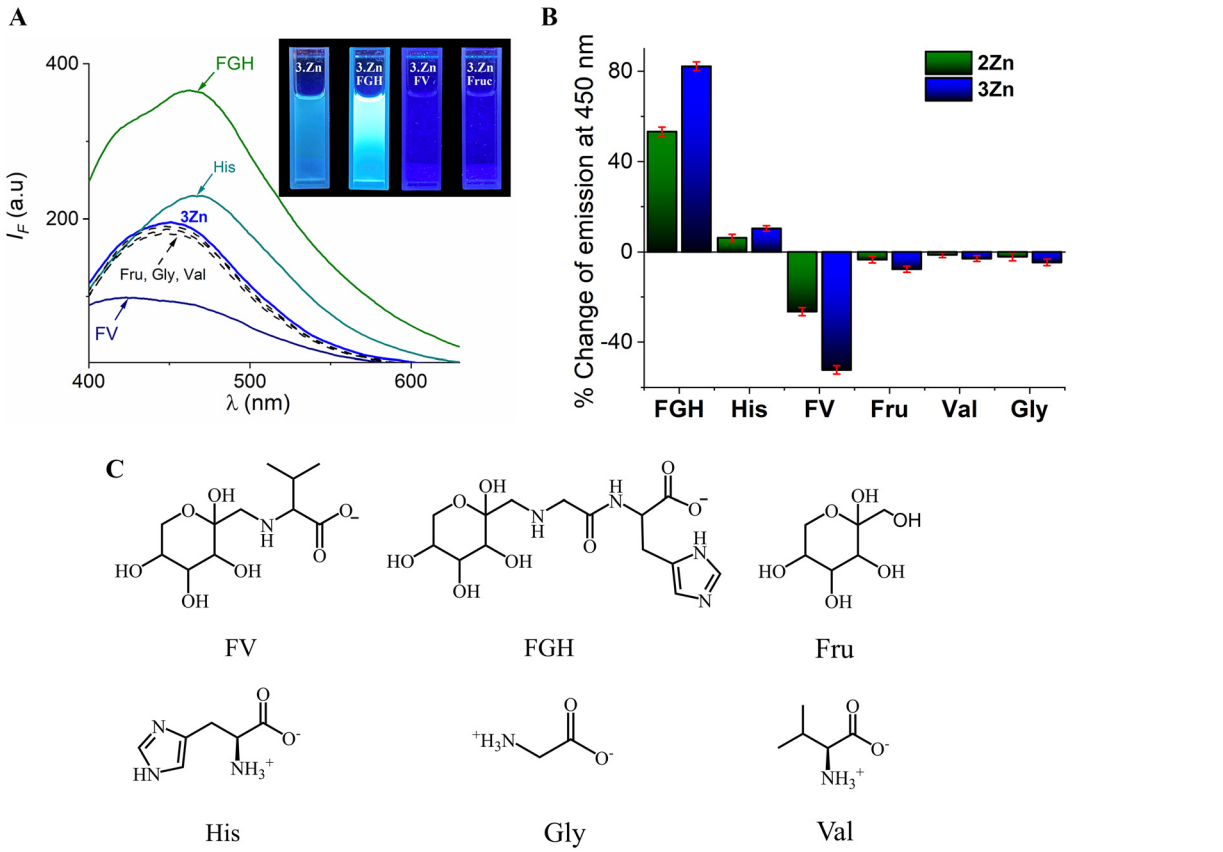

Fig. 6 (A) Changes in fluorescence spectra (λ_{ex} = 330 nm) and (B) percentage changes in fluorescence intensity at 450 nm of **2Zn** and **3Zn** (20 μM) in buffered solution (10 mM MOPS pH = 7.4) upon the addition FV, FGH, Fru, Gly, Val and His ($[analyte]_{total}$ = 100 μM), average of triplicate experiments. (C) Analytes used in this work.

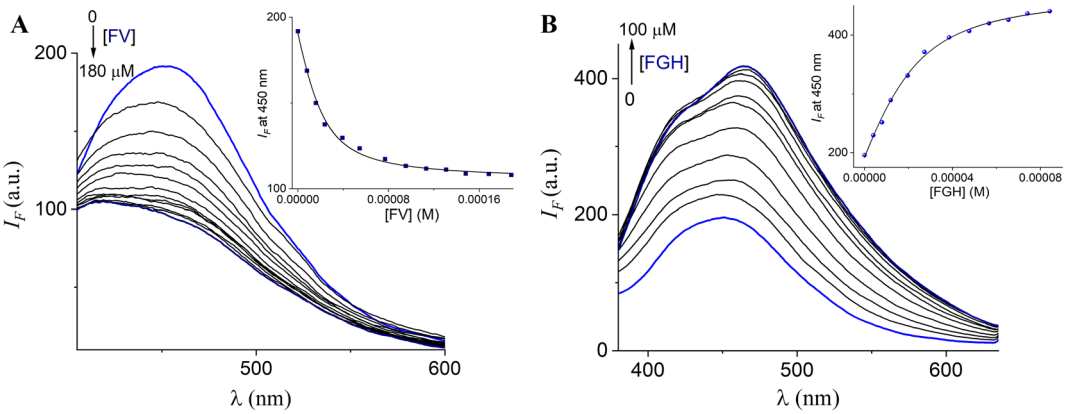

Fig. 7 Changes in the emission spectra (λ_{ex} = 330 nm) of buffered (10 mM, MOPS, pH = 7.4) aqueous solutions of **3Zn** (20 μM) upon the addition of increasing amounts of (A) FV and (B) FGH. The inset shows the curve at 450 nm (average of triplicate experiments). The solid line was obtained by fitting to eqn (1).

Although Val or His have potential metal binding sites (carboxylate/imidazole) and Fru can interact with boronic acid, these seem to only involve the recognition of one point with the Zn-complexes.

Reversible two-point recognition with derivatives of Zn complexes bearing a phenylboronic acid has been used in binding flexible biological polyol-appended carboxylic acids such as sialic acid[59] and uronic acid.[61]

To support the two-point recognition mechanism we estimated the affinity constant of FV and FGH towards the reference compound **5Zn** which lacks boronic acid under the same conditions (Fig. 8C and D). In both cases, the affinity and

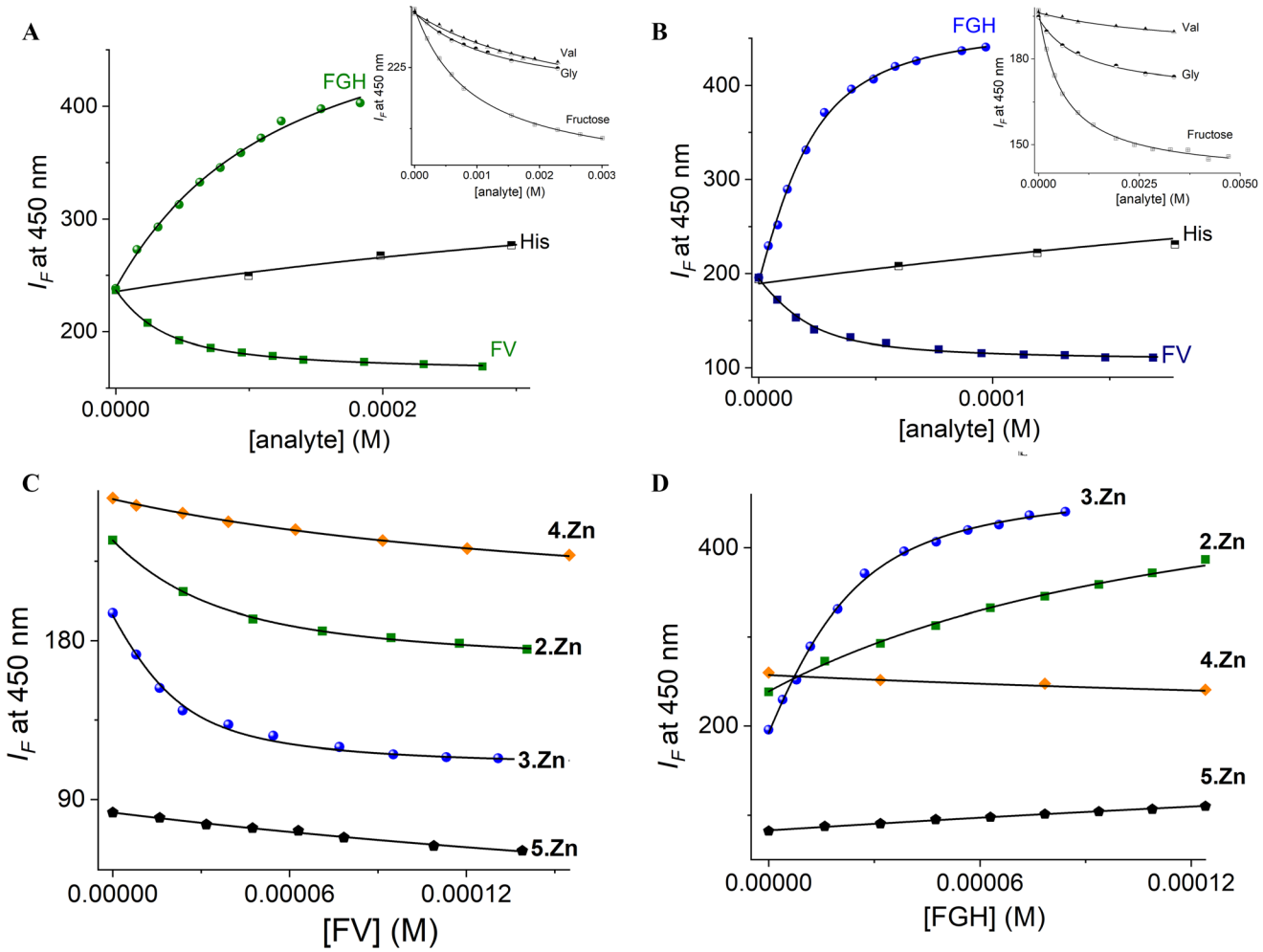

Fig. 8 Fluorimetric titration (λ_{ex} = 330 nm) of aqueous solutions of (A) **2Zn** and (B) **3Zn** (20 μM) upon the addition of increasing amounts of fructosyl amino acids, His, Gly, Val and fructose at pH 7.4. The solid lines were obtained by fitting to eqn (1). Fluorimetric titration profiles of all Zn-complexes with (C) FV and (D) FGH.

Table 3 Apparent binding constants K (M^{-1}) for Zn-complexes (20 μM) with fructosyl amino acids and some comparative analytes in buffered aqueous solutions at pH = 7.4

Analyte	**2Zn**, $K_{(1:1)}$	**3Zn**, $K_{(1:1)}$	**4Zn**, $K_{(1:1)}$	**5Zn**, $K_{(1:1)}$
FV	$(4.16 \pm 0.10) \times 10^4$	$(1.43 \pm 0.10) \times 10^5$	$(2.89 \pm 0.09) \times 10^3$	$(2.39 \pm 0.13) \times 10^3$
FGH	$(9.07 \pm 0.07) \times 10^3$	$(1.02 \pm 0.07) \times 10^5$	$(2.58 \pm 0.11) \times 10^3$	$(1.23 \pm 0.11) \times 10^3$
His	$(1.28 \pm 0.09) \times 10^3$	$(1.41 \pm 0.08) \times 10^3$	$(8.02 \pm 0.12) \times 10^2$	—[a]
Gly	$(7.19 \pm 0.07) \times 10^2$	$(9.24 \pm 0.09) \times 10^2$	$(6.28 \pm 0.06) \times 10^2$	—[a]
Val	$(3.55 \pm 0.12) \times 10^2$	$(2.66 \pm 0.12) \times 10^2$	$(3.27 \pm 0.07) \times 10^2$	—[a]
Fru	$(1.10 \pm 0.03) \times 10^3$	$(1.68 \pm 0.07) \times 10^3$	$(1.25 \pm 0.12) \times 10^3$	—[a]

[a] Not calculated.

effect on the intensity are like that observed for pure amino acids (Val or His) and drops three orders of magnitude when compared to the affinity between the fructosyl amino acids and **3Zn**.

On the other hand, the affinity of **3Zn** and **2Zn** towards FV in the range of K = (1.43–0.41) × 10^5 M^{-1} is considerably greater than the stability constant of phenylboronic acid and Fru (K = 160 M^{-1}, taken from the literature)[25] which is consistent with (1) the increase of stability of the boronate–diol interaction promoted by the strong Lewis acidity of the phenylboronic groups in these Zn-complexes and (2) the participation of interaction carboxylate-metal as a cooperative binding site.

From the data in Table 3, the order of preference of FV/FGH towards the receptors is **3Zn** > **2Zn** > **4Zn** which correlates with the acidity of their $-B(OH)_2$ groups. This correlation strongly indicates that the diol binding boronic acid site drives the

interaction between Zn-complexes and studied fructosyl amino acids as evidenced by ^{11}B NMR measurements. Among Zn-complexes, the most efficient receptor **3Zn** binds FV about 1.5 times more tightly than does FGH, probably due to the electrostatic contribution of the carboxylate anion from Val.

In order to explore the nature of the fluorescence response induced by fructosyl amino acids, the lifetimes of **3Zn** in the absence and presence of FV and FGH were recorded. An aqueous solution of **3Zn** upon excitation with a 354 laser displayed a bi-exponential decay with lifetimes τ_1 = 4.70 ns and τ = 0.08 ns (Fig. 9).

The **3Zn** complex with 3.0 equiv. of FV exhibited a biexponential decay with nearly similar values, τ_1 = 3.98 ns and τ = 0.06 ns, suggesting a mainly static quenching by complexation (**3Zn**–FV) as evidenced by NMR, ESI-MS and UV-Vis experiments.

It is well known that a static quenching mechanism in a system fluorophore–quencher does not change the lifetime values.[62] In contrast, the addition of FGH modestly increases the lifetimes up to τ_1 = 6.10 ns and τ_2 = 1.38 ns. These longer values can be ascribed to the disappearance of any non-emitting charge transfer caused by the coordination of the imidazole ring as well as the formation of a large rigid extended π-conjugated system involving ligand–ligand charge transfers in the final coordination complex.[63]

Considering all foregoing spectroscopic evidence, the crystal structure and ESI-MS results, the molecular recognition modes of **3Zn** with fructosyl amino acids are illustrated in Fig. 10. Therein, **3Zn** can complex with FV or FGH through two-point recognition, one diol-binding boronic acid site and the other at the carboxylate anion or imidazole ring binding Zn atom. According to the best of our knowledge, this is the first example of an artificial fluorescent receptor for fructosyl amino acids and the sole for FV.

The reversibility of the boronic acid–diol interaction is a key aspect of molecular recognition because it serves as a basis for understanding and improving the sensing response of the target analyte,[28,33] therefore, we investigated the reversibility of

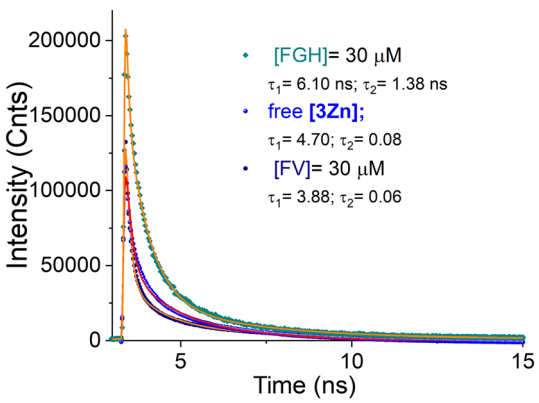

Fig. 9 Emission decay profiles of aqueous solutions of **3Zn** (10 μM) in the absence and presence of 3.0 equiv. of FV and FGH at pH = 7.4. The solid lines were obtained by fitting to bi-exponential decays.

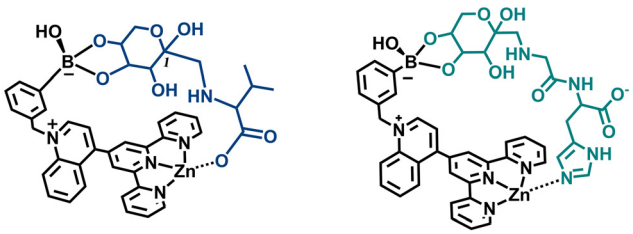

Fig. 10 The complexation mode proposed for binding of the two-points of FV and FGH to the **3Zn** complex.

the interaction of **3Zn** with FV through a qualitative experiment using the Alizarin Red S (ARS) dye.

It is well known that ARS binds reversibly to arylboronic acids and is commonly used for the formation of dynamic chromogenic assemblies with application in the detection of saccharides.[25,64]

In a typical experiment, an aqueous solution of ARS displays a dramatic change in color in response to the binding of a boronic acid from deep red to yellow. The displacement of the maxima occurs from ~520 cm (free ARS, deep red) to ~460 cm (ARS + boronic acid, yellow) as described in detail by Wang.[25]

We initially monitored the color change of free ARS (100 mM) upon the addition of our complex containing the boronic acid, **3Zn** (1.1 equiv.) in a buffered aqueous solution at pH = 7.4. As shown in Fig. S49,† there is a hypsochromic shift in the maxima, from 521 nm to 458 nm, similar to that reported for the ARS–boronic acid systems, induced by the formation of the sp^3 boronic ester. Subsequently, the addition of an excess of FV (10 equiv.) practically restored the spectrum of free ARS both in its form and at its maximum, suggesting that the ARS dye was displaced by the FV analyte which shows the reversibility of the ARS–**3Zn** complex.

Furthermore, the reversibility of the supramolecular **3Zn**–FV complex qualitatively was verified as described below.

The complex prepared *in situ* **3Zn**–FV (110 μM, each component) was added to an aqueous buffered solution of ARS (100 μM) and as seen in Fig. S50,† the initial absorption maximum at 520 nm was displaced to 461 nm, corresponding to the formation of the ARS–**3Zn** complex, which is only possible if the dye displaces the FV analyte. These experiments provide strong evidence of reversibility in the complexation of the molecular receptor **3Zn** with FV in water.

DFT calculation

Finally, to gain further insight into the cooperative binding mode of **3Zn** with FV and FGH, density functional theory calculations were carried out for the 1 : 1 supramolecular complexes. All calculations were carried out with the Gaussian16 suite of programs[65] at the ωB97-XD/LANL2DZ level of theory with the PCM implicit solvent model (water). Thus, complexes **3Zn**–FV and **3Zn**–FGH were optimized in order to assess their coordination preferences (Fig. 11). Frequency calculations

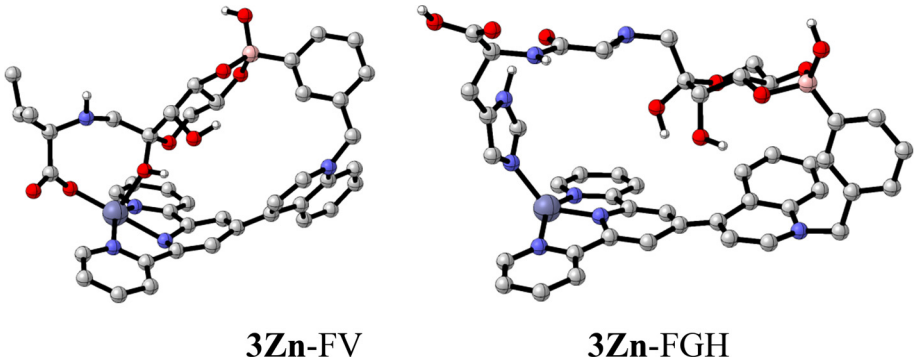

Fig. 11 Optimized structures of **3Zn**–FV and **3Zn**–FGH at the ωB97-XD/LANL2DZ level of theory (hydrogen atoms not shown for clarity).

reveal both compounds to be minimal on their respective potential energy surfaces.

FV is long enough to coordinate with two –OH groups of the fructose moiety with the tetrahedral sp^3-boronate anion and cooperatively coordinate with the carboxylate group from Val with the Zn atom.

Additionally, a close (Fru)C1–OH···Zn interaction is observed which generates a pentacoordinate Zn complex. Therefore, a three-point recognition between **3Zn** and FV is sketched, which may explain their high affinity.

On the other hand, a bent conformation of FGH interacts with **3Zn** through the boronate ester with two OH groups from the Fru moiety and a coordination bond between the imidazole ring and the metallic atom to give a tetracoordinated Zn complex. Thermochemistry calculations derived from the vibrational analysis reveals that **3Zn**–FV is more stable than compound **3Zn**–FGH by ~11.24 kcal mol^{-1}, which makes the former the best candidate for a receptor from a theoretical standpoint. The B···Zn distances for the optimized structures are 9.79 Å and 10.59 Å for **3Zn**–FV and **3Zn**–FGH, respectively. These values are close to the B···Zn distance in the crystal structure (12.44 Å). The narrowing of the B···Zn distance in the receptor induced by the coordination of the fructosyl amino acids is plausible due to the flexible methylene group of the receptor that can rotate and bring these atoms closer together.

Conclusions

We have described the first example of a set of fluorescent Zn-terpyridine complexes appended to strongly acidified phenylboronic acid groups for optical recognition of biochemically relevant fructosyl amino acids that occur in HbA1c such as FV and FGH.

These cationic Zn-complexes possess a high-water solubility, photostability and strong ability for fluorescence sensing of FV and FGH in a micromolar concentration range at physiological pH.

The complex bearing *meta*-substituted boronic acid **3Zn** stood out from the other two (*ortho*-**2Zn** and *para*-**4Zn**) for having the most acidic $-B(OH)_2$ group with pK_a = 6.98 and exceptionally strong affinity for FV (K = 1.43 × 10^5 M^{-1}) and FGH (K = 1.05 × 10^5 M^{-1}) with selectivity over their separate molecular constituents such as fructose, Val, Gly and His.

^{1}H, ^{11}B NMR, UV-Vis and fluorescence titration experiments, MS measurements, X-ray crystal structure and DFT calculations showed that FV and FGH are bound to **3Zn** in a 1 : 1 mode through two-point recognition that involves (1) a boronate–diol complexation and (2) the coordination bond of the carboxylate anion (FV) or the imidazole ring (FGH) to the Zn atom.

Addition of FV to an aqueous solution of **3Zn** displays an efficient quenching response which can be explained by a static PET mechanism possibly in both the excited and the ground state as evidenced by lifetime measurements and spectroscopic titrations. In contrast, addition of FGH induced a notable turn-on signal which can be rationalized by a rigidification of the complex and a decrease in the hydration grade of the final **3Zn**–FGH complex.

Overall, these results further highlight the usefulness of a new set of water-soluble and fluorescent receptors based on two different Lewis acids as analytical tools for the selective and direct sensing of fructosyl amino acids with biochemical and medical relevance.

Experimental section

General conditions, chemicals and equipment are described in the ESI.† Isomers **2–4** and compound **5** were prepared according to a modified methodology reported previously.[50]

Chemical synthesis

Synthesis of compound 1, 4-([2,2′:6′,2″-terpyridin]-4′-yl)quinoline. 2-Acetylpyridine (308.4 mg, 285.0 μL, 2.6 mmol) was dissolved in an ethanolic solution (35.0 ml) of KOH (500.0 mg, 8.90 mmol) in a balloon flask and it was vigorously stirred for 10.0 min, separately, 4-quinolinecarboxaldehyde (200.20 mg, 1.30 mmol) was dissolved in EtOH (10.0 mL) and added drop

by drop to the 2-acetylpyridine basic solution. The reaction mixture was stirred for ~20 min at r.t., and then aqueous NH_3 (10.5 ml, 12.5 mmol, 29.50%) was added and refluxed for 48 h under a N_2 atmosphere.

The solvent was reduced under vacuum up to ~20% of the initial volume and cold distilled water (60.0 mL) was added to give a precipitate. This precipitate was filtered off, washed with water twice (5.0 mL) and recrystallized in EtOH to obtain **1** as pale pink crystalline powder. Yield: 344.0 mg (75.0%).

^{1}H NMR (300 MHz, 25 °C, DMSO-d_6) δ (ppm) 9.05 (d, J = 6.37 Hz, 1H), 8.74–8.70 (m, 4H), 8.56 (s, 2H), 8.18 (d, J = 8.32 Hz, 1H), 8.07 (m, 2H), 7.93 (dd, J = 8.56, 1.36 Hz, 1H), 7.86 (m, 1H), 7.69–7.63 (m, 2H), 7.53 (m, 2H).

^{13}C NMR (75 MHz, 25 °C, DMSO-d_6) δ (ppm) 155.54, 154.67, 150.45, 149.52, 148.16, 147.39, 145.07, 137.68, 129.96, 129.84, 127.72, 125.11, 124.85, 121.42, 121.16, 121.04 (one signal was not detected).

ESI(+)-MS (m/z) $[\mathbf{1}]^+$: calculated for $[C_{24}H_{17}N_4]^+$: 361.15, found: 361.30. Anal. calcd for $C_{24}H_{16}N_4$ (360.42); C, 79.98; H, 4.47; N, 15.15. Found: C, 79.97; H, 4.56; N, 15.04.

Synthesis of ligand 2, 4′-[*N*-(2-boronobenzyl)-4-quinolinium]-2,2′:6′,2″-terpyridine bromide. **1** (100.0 mg, 0.28 mmol) and 1.1 equiv. of 2-(bromomethyl)phenylboronic acid (72.86 mg, 0.31 mmol) were dissolved in anhydrous CH_3CN (75.0 mL) and refluxed for 72 h under a N_2 atmosphere. The solvent was removed under reduced pressure, and then ethyl acetate (40.0 mL) was added and stirred for 1 h at r.t. The precipitate formed was filtered off, washed with Et_2O twice (5 mL), and dried under vacuum for ~3 h to furnish **2** as a crystalline beige solid. Yield: 127.7 mg (80.0%).

^{1}H NMR (300 MHz, 25°, DMSO-d_6) δ (ppm) 9.62 (d, J = 6.14 Hz, 1H), 8.79 (d, J = 7.73 Hz, 2H), 8.75–8.70 (m, 4H), 8.62–8.50 (m, 2H), 8.44 (d, J = 6.04 Hz, 1H), 8.29–8.18 (m, 2H), 8.11 (m, 2H), 8.01 (t, J = 7.68 Hz, 1H), 7.87 (dd, J = 7.16, 1.65 Hz, 1H), 7.58 (m, 2H), 7.43–7.29 (m, 3H), 6.85 (d, J = 7.72 Hz, 1H), 6.63 (s, 2H).

^{13}C NMR (126 MHz, 25 °C, DMSO) δ (ppm) 156.04, 155.61, 154.26, 149.74, 149.52, 145.19, 138.40, 137.89, 135.56, 135.43, 134.05, 130.63, 130.40, 128.18, 127.89, 127.72, 126.50, 125.12, 122.74, 121.26, 120.95, 119.90, 60.85 (one signal was not detected).

ESI(+)-MS (m/z): calculated for $[C_{31}H_{24}BN_4O_2]^+$: 495.20, found: 495.20. ATR-IR ν (cm^{-1}): 3329br, 3055m, 1579m, 1366s, 764s.

Synthesis of ligand 3, 4′-[*N*-(2-boronobenzyl)-4-quinolinium]-2,2′:6′,2″-terpyridine bromide. **1** (100.0 mg, 0.28 mmol) and 1.10 equiv. of 3-(bromomethyl)phenylboronic acid (72.94 mg, 31 mmol) were dissolved in anhydrous CH_3CN (70 mL) and refluxed for 72 h with a N_2 atmosphere. Then, the solvent was removed under reduced pressure and ethyl acetate (40 mL) was added. The mixture was stirred for 5 h. Finally, the solid was filtered off, washed with Et_2O twice (5 mL) and dried under vacuum for ~3 h to give **3** as pale beige powder. Yield: 135.7 mg, (85.0%).

^{1}H NMR (300 MHz, 25 °C, DMSO-d_6) δ (ppm) 9.86 (d, J = 5.89 Hz, 1H), 8.78 (d, J = 7.38 Hz, 2H), 8.76–8.68 (m, 4H), 8.57 (d, J = 9.61 Hz, 1H), 8.51 (d, J = 6.00 Hz, 1H), 8.30–8.21 (m, 2H), 8.17 (s, 2H), 8.10 (m, 2H), 8.00 (t, J = 7.73 Hz, 1H), 7.82–7.75 (m, 2H), 7.57 (m, 2H), 7.48–7.36 (m, 2H), 6.48 (s, 2H).

^{13}C NMR (101 MHz, 25 °C, DMSO-d_6) δ (ppm) 156.31, 155.69, 154.33, 150.01, 149.58, 148.07, 145.17, 138.11, 137.88, 135.63, 134.49, 133.07, 132.61, 130.72, 128.93, 128.30, 128.07, 125.14, 122.93, 121.28, 120.97, 120.04, 60.46, (one signal was not detected).

ESI(+)-MS (m/z): calculated for $[C_{31}H_{24}BN_4O_2]^+$: 495.20, found: 495.2. ATR-IR ν (cm^{-1}): 3309br, 3058m, 2960w, 1579m, 1368m, 1329m, 707m.

Synthesis of ligand 4, 4′-[*N*-(4-boronobenzyl)-4-quinolinium]-2,2′:6′,2″-terpyridine bromide. This isomer was obtained following the same procedure as that for **3**, from 4-(bromomethyl)phenylboronic acid instead of 3-(bromomethyl)phenylboronic acid. Yield: 140.5 mg, (88%).

^{1}H NMR (301 MHz, 25 °C, DMSO-d_6) δ (ppm) 9.86 (d, J = 6.15 Hz, 1H), 8.78 (d, J = 7.92 Hz, 2H), 8.75–8.70 (m, 4H), 8.56–8.47 (m, 2H), 8.28–8.19 (m, 2H), 8.16 (s, 2H), 8.11 (m, 2H), 7.99 (t, J = 7.79 Hz 1H), 7.81 (d, J = 8.17 Hz, 2H), 7.57 (m, 2H), 7.37 (d, J = 8.04 Hz, 2H), 6.48 (s, 2H). ^{13}C NMR (126 MHz, 25 °C, DMSO-d_6) δ (ppm) 156.40, 155.62, 154.32, 150.04, 149.53, 145.20, 138.04, 137.83, 135.78, 135.53, 134.76, 130.63, 128.25, 128.11, 126.04, 125.09, 122.96, 121.24, 120.97, 120.28, 119.98, 60.28.

ESI(+)-MS (m/z): calculated for $[C_{31}H_{24}BN_4O_2]^+$: 495.2, found: 495.2. ATR-IR ν (cm^{-1}): 3313br, 3058m, 1567s, 1367m, 1334m, 1015m, 765m.

Synthesis of ligand 5, 4′-[*N*-(benzyl)-4-quinolinium]-2,2′:6′,2″-terpyridine bromide. **1** (80.0 mg, 0.22 mmol) and 2.0 equiv. of benzyl bromide (54.0 μL, 0.45 mmol) were dissolved in anhydrous CH_3CN (70 mL) and refluxed for 24 h with a N_2 atmosphere. The solvent was removed under reduced pressure, ethyl acetate (40.0 mL) was added and left stirring for ~3 h at r.t. The solid was filtered under vacuum, and crystallized in an EtOH–acetone (1 : 1, v/v) system, obtaining white needle-shaped crystals. Yield: 94.4 mg (60%).

^{1}H NMR (300 MHz, 25 °C, DMSO-d_6) δ (ppm) 9.90 (d, J = 6.07 Hz, 1H), 8.79 (d, J = 7.94 Hz, 2H), 8.74–8.72 (m, 2H), 8.72 (s, 2H), 8.59 (d, J = 9.04 Hz, 1H), 8.51 (d, J = 5.98 Hz, 1H), 8.27–8.23 (m, 2H), 8.11 (m, 2H), 8.00 (m, 1H), 7.58 (m, 2H), 7.46–7.37 (m, 5H), 6.51 (s, 2H). ^{13}C NMR (126 MHz, DMSO-d_6) δ (ppm) 156.37, 155.61, 154.30, 150.00, 149.52, 145.16, 138.01, 137.81, 135.55, 134.07, 130.64, 129.10, 128.73, 128.25, 128.10, 127.13, 125.08, 122.93, 121.22, 120.93, 119.96, 60.13.

MALDI(+)-TOF (m/z): calculated for $[C_{31}H_{23}N_4]^+$: 451.19, found: 452.351. ATR-IR ν (cm^{-1}): 3381br, 3056m, 2954m, 1732s, 1580s, 1370m, 1236s, 745m.

General synthesis path for the Zn-complexes

The corresponding ligand **2–4** and 1.10 equiv. of the $ZnBr_2{\cdot}2H_2O$ salt were placed in a balloon flask with 5.0 mL of the mixture EtOH : CH_3CN (1 : 1, v/v). The reaction mixture was stirred for 24 h at r.t. to give a white solid, (in all cases). The solvents were removed under reduced pressure, the precipitate was washed twice with cold EtOH (10 mL) and dried under

vacuum for ~2 h to give the bromide salt of the corresponding Zn(II) complex.

Synthesis of complex 2Zn. Following the general path, the ligand **2** (43.0 mg, 0.08 mmol) and $ZnBr_2{\cdot}2H_2O$ (23.86 mg, 0.90 mmol) were reacted to obtain **2Zn**. Yield: 52.7 mg, (88.0%).

^{1}H NMR (300 MHz, 25 °C, DMSO-d_6) δ (ppm) 9.76 (d, J = 5.07 Hz, 1H), 9.19 (s, 2H), 8.94 (s, 2H), 8.78 (d, J = 8.00 Hz, 2H), 8.66–8.62 (m, 2H), 8.55 (d, J = 5.75 Hz, 2H), 8.47 (d, J = 8.50 Hz, 1H), 8.37 (t, J = 7.58 Hz, 2H), 8.31 (t, J = 7.98 Hz, 1H), 8.04 (t, J = 7.67 Hz, 1H), 7.98–7.91 (m, 2H), 7.92 (d, J = 7.29 Hz, 1H), 7.45–7.35 (m, 2H), 6.81 (d, J = 7.66 Hz, 1H), 6.70 (s, 2H).

^{13}C NMR (75 MHz, 25 °C, DMSO-d_6) δ (ppm) 149.73, 149.53, 148.97, 148.80 (shoulder), 146.33, 140.90, 138.22, 137.60, 135.99, 135.63, 135.40, 130.93, 130.42, 130.22, 128.91, 127.94, 127.79, 127.53, 123.82, 123.00, 122.81, 119.80, 60.96. ^{11}B NMR (96 MHz, 25 °C, CD_3OD–DMSO-d_6, 4 : 1, v/v) δ (ppm) 28.62.

ESI(−)-MS (m/z): calculated $[C_{31}H_{24}BBr_4N_4O_2Zn]^-$: 880.81, found: 880.5. ESI(+)-MS (m/z): calculated $[C_{31}H_{26}BBr_2N_4O_3Zn]^+$: 738.98, found: 739.0. ATR-IR ν (cm^{-1}): 3324br, 3056m, 1597s, 1367s, 763s, 637m. Far IR ν (cm^{-1}): 408m, 315w, 202br, 171s. Anal. calcd for $C_{31}H_{24}BBr_3N_4O_2Zn$ (800.46); C, 46.52; H, 3.02; N, 7.00. Found: C, 46.97; H, 3.36; N, 6.84.

Synthesis of complex 3Zn. Following the general path, the ligand **3** (50.0 mg, 0.08 mmol) and $ZnBr_2{\cdot}2H_2O$ (23.86 mg, 0.09 mmol) were reacted to obtain **3Zn**. Single crystals for X-ray diffraction of **5Zn** were obtained by slow solvent evaporation from a CH_3CN/EtOH (1 : 1, v/v) solution after 4 days at low temperature (~4 °C). Yield: 64.0 mg, (92%).

^{1}H NMR (300 MHz, 25 °C, DMSO-d_6) δ (ppm) 10.11 (d, J = 5.91 Hz, 1H), 9.18 (s, 2H), 8.93 (d, J = 4.34 Hz, 2H), 8.79–8.70 (m, 4H), 8.62 (d, J = 5.75 Hz, 1H), 8.47 (d, J = 8.59 Hz, 1H), 8.40–8.30 (m, 3H), 8.20 (s, 2H), 8.03 (t, J = 7.79 Hz, 1H), 7.99–7.89 (m, 2H), 7.83 (d, J = 7.29 Hz, 1H), 7.54 (d, J = 7.78 Hz, 1H), 7.43 (t, J = 7.50 Hz, 1H), 6.53 (s, 2H).

^{13}C NMR (126 MHz, DMSO-d_6) δ (ppm) 154.43, 150.09, 149.52, 149.02, 148.91, 146.37, 140.98, 137.88, 136.09, 135.37, 134.71, 133.11, 132.95, 131.05, 129.28, 129.07, 128.35, 127.86, 127.77, 123.90, 123.18, 122.84, 120.01, 60.71. ^{11}B NMR (96 MHz, 25 °C, CD_3OD–DMSO-d_6, 4 : 1, v/v) δ (ppm) 28.50.

ESI(−)-MS (m/z): calculated $[C_{31}H_{24}BBr_4N_4O_2Zn]^-$: 880.81, found: 880.2. ESI(+)-MS (m/z): calculated $[C_{31}H_{24}BBr_2N_4O_2Zn]^+$: 720.97, found: 720.4. ATR-IR ν (cm^{-1}): 3397br, 3064m, 2972w, 1599s, 1368s, 1333s, 1014m, 764s, 706s, 637m. Far IR ν (cm^{-1}): 410w, 209br, 171m. Anal. calcd for the X-ray single crystal sample $C_{33}H_{34}BBr_3N_4O_5Zn$ (882.54); C, 44.91; H, 3.88; N, 6.35. Found: C, 44.96; H, 3.93; N, 6.32.

Synthesis of complex 4Zn. Following the general path, the ligand **4** (50.0 mg, 0.08 mmol) and $ZnBr_2{\cdot}2H_2O$ (25.23 mg, 0.09 mmol) were reacted to obtain **4Zn**. Yield: 62.6 mg, (90.0%).

^{1}H NMR (300 MHz, 25° C, DMSO-d_6) δ (ppm) 10.09 (d, J = 4.87 Hz, 1H), 9.18 (s, 2H), 8.95 (s, 2H), 8.80–8.67 (m, 3H), 8.61 (d, J = 5.33 Hz, 1H), 8.48–8.28 (m, 4H), 8.15 (s, 2H), 8.06–7.93 (m, 3H), 7.83 (d, J = 7.96 Hz, 2H), 7.44 (d, J = 7.33 Hz, 2H), 6.54 (s, 2H). ^{13}C NMR (75 MHz, 25 °C, DMSO-d_6) δ (ppm) 154.51, 150.16, 149.49, 148.99, 148.85, 146.35, 140.94, 137.79, 136.04, 135.56, 134.80, 131.00, 129.02, 127.80, 126.36, 123.83, 123.14, 122.77, 121.41, 119.96, 115.86, 60.53. ^{11}B NMR (96 MHz, 25 °C, CD_3OD–DMSO-d_6, 4 : 1, v/v) δ 28.73.

ESI(−)-MS (m/z): calculated $[C_{31}H_{24}BBr_4N_4O_2Zn]^-$: 880.81, found: 880.5. ATR-IR ν (cm^{-1}): 3346br, 3057m, 3032m, 1598s, 1366s, 1334s, 1013s, 792s, 636s. Far IR ν (cm^{-1}): 410m, 209br, 197br, 177m. Anal. calcd for $C_{31}H_{24}BBr_3N_4O_2Zn$ (800.46); C, 46.52; H, 3.02; N, 7.00. Found: C, 46.82; H, 3.27; N, 6.95.

Synthesis of complex 5Zn. Complex **5Zn** was obtained following the general procedure; the ligand **5** (60.0 mg, 0.11 mmol) and $ZnBr_2{\cdot}2H_2O$ (32.7 mg, 0.12 mmol) were used to prepare **5Zn**, which was obtained as a crystalline white powder. Single crystals of **5Zn** for X-ray diffraction were obtained by slow solvent evaporation from a CH_3CN/EtOH (1 : 1, v/v) solution after 7 days at r.t. Yield: 55.5 mg, (68%).

^{1}H NMR (301 MHz, 25 °C, DMSO-d_6) δ (ppm) 9.90 (d, J = 6.07 Hz, 1H), 8.79 (d, J = 7.94 Hz, 2H), 8.74–8.72 (m, 2H), 8.72 (s, 2H), 8.59 (d, J = 9.04 Hz, 1H), 8.51 (d, J = 5.98 Hz, 1H), 8.27–8.23 (m, 2H), 8.11 (td, J_{HH} = 7.75, 1.80 Hz, 2H), 8.00 (m, 1H), 7.58 (m, 2H), 7.46–7.37 (m, 5H), 6.51 (s, 2H). ^{13}C NMR (126 MHz, DMSO-d_6) δ (ppm) 156.37, 155.61, 154.30, 150.00, 149.52, 145.16, 138.01, 137.81, 135.55, 134.07, 130.64, 129.10, 128.73, 128.25, 128.10, 127.13, 125.08, 122.93, 121.22, 120.93, 119.96, 60.13.

ESI(−)-MS (m/z): calculated for negative scan $[C_{31}H_{23}Br_4N_4Zn]^-$: 836.79, found: 836.5. ESI(+)-MS (m/z): calculated $[C_{31}H_{23}Br_2N_4Zn]^+$: 676.9, found: 676.8. ATR-IR ν (cm^{-1}): 3381br, 3056m, 2954m, 1732s, 1580s, 1370m, 1236s, 745m. Anal. calcd for $C_{31}H_{23}Br_3N_4Zn$ (756.65); C, 49.21; H, 3.06; N, 7.40. Found: C, 49.53; H, 3.39; N, 7.24.

Synthesis of fructosyl valine (FV). FV was obtained according to the methodology previously reported.[24] The purity of FV was verified by ^{1}H and ^{13}C NMR spectroscopy, ESI-MS and elemental analysis. All analytical data including MS were consistent with the data reported.[8]

^{1}H NMR (300 MHz, 25 °C, DMSO-d_6) δ 4.09–4.00 (m, 2H), 3.96–3.87 (m, 1H), 3.81 (s, 1H), 3.77 (s, 1H), 3.67 (d, J_{HH} = 4.21 Hz, 1H), 3.34 (s, 2H), 2.31 (m, 1H), 1.07 (dd, J_{HH} = 20.97, 6.91 Hz, 6H). ^{13}C NMR (76 MHz, D_2O) δ (ppm) 172.20, 95.25, 70.12, 69.32, 69.04, 68.87, 63.86, 53.34, 29.02, 18.45, 16.90.

ESI-MS (m/z): calculated for $[C_{11}H_{22}NO_7]^+$: 280.14, found: 280.2. ATR-IR ν (cm^{-1}): 3449m, 3417m, 3212w, 2966s, 2903w, 1569s, 1328s, 1084s, 762m, 562s. M.p. 155 °C (from the literature 154 °C).

Synthesis of fructosyl glycyl histidine (FGH). FGH was obtained following the same procedure as that for FV, from dipeptide glycyl L-histidine (Gly-His, Aldrich G1627) instead L-valine, with 60% yield. The identity and purity were verified by high-resolution spectrometry of ESI and NMR spectroscopy. All data including the experimental pattern of isotope distribution matches well with the theoretical isotopic distribution of FGH.

^{1}H NMR (300 MHz, 25 °C, D_2O) δ 8.59 (s, 1H), 7.29 (s, 1H), 4.56 (m, 1H), 4.12–3.54 (m, 7H), 3.52–2.94 (m, 4H). ^{13}C NMR (101 MHz, D_2O) δ (ppm) 176.41, 133.74, 133.41, 130.25,

116.91, 69.43, 68.97, 63.62, 57.40, 54.23, 49.73, 27.62, 27.36, 16.74. HRMS-ESI$^+$ (m/z): calculated for $[C_{14}H_{23}N_4O_8]^+$: 375.15, found: 375.150916. ATR-IR ν (cm^{-1}): 3258br, 3144br, 2879m, 1588s, 1391s, 1078m, 1028m, 623br, 532br.

Fluorescence experiments and lifetime measurements

Titration experiments were carried out by adding aliquots of stock solutions of the analyte to a neutral aqueous solution (10 mM of MOPS, pH 7.4) of the corresponding Zn-complex (20 μM). After the addition of analytes, the solution was equilibrated for 1 min at r.t. before recording the emission spectrum (λ_{ex} = 330 nm) using a quartz cuvette. Lifetime measurements were made according to ref. 62 and the details are described in the ESI.†

^{11}B, ^{1}H NMR titration experiments

NMR titration experiments were performed using a 300 MHz spectrometer. ^{11}B NMR spectra were recorded at 96 MHz. Aliquots of concentrated stock solutions of FGH were added directly to the corresponding Zn-complex (10 mM) solution in CD_3OD–DMSO-d_6 (v/v, 4/1) at 25 °C using quartz NMR tubes. In the case of ^{1}H NMR experiments, the spectra were recorded after the addition of aliquots of a concentrated solution of **3Zn** to FHG solution in CD_3OD, directly in an NMR tube.

Crystallographic experiments

The relevant details of the crystals **3Zn** and **5Zn**, data collection and structure refinement can be found in Table S1.† These single-crystals were collected on a Bruker APEX II CCD diffractometer at 100 K, using Cu-K$_\alpha$ radiation (k = 1.54178 Å) from an Incoatec ImuS source and Helios optic monochromator.[66] Suitable single-crystals were coated with hydrocarbon oil, picked up with a nylon loop, and mounted in the cold nitrogen stream of the diffractometer. The structures were solved by direct methods[67] and refined by full-matrix least-squares on F^2 using the ShelXle GUI.[68,69]

The hydrogen atoms of the C–H and O–H bonds were placed in idealized positions, as it was not possible to find the hydrogen atoms from the O–H moiety in the map of residual density, and their position was refined with $U_{iso} = aU_{eq}$, where a is 1.5 for –CH_3 and –OH moieties and 1.2 for others.

The disorder moieties in complexes **3Zn** and **5Zn** were modeled using RIGU, SIMU, SAME and EADP instructions described in SHELXL.[67] For complex **3Zn**, the molecule of ethanol exhibits positional disorder with an 85/15 occupancy ratio between the two positions, while the bromide anion is modeled in 2 positions with 95/5 occupancy ratio. For complex **5Zn**, the occupancy where three or more positions are modeled was obtained using free variables and the sump instruction and subsequently set to restrict to unity. The asymmetric unit consists of three independent molecules, in the first molecule the positional disorder of a benzene ring was modeled, in the second and third molecule the positional disorder of pyridine rings was modeled; in all cases two positions were modeled using the same free variable, with a 63/37 occupancy ratio between the two positions, the anion $[ZnBr_4]^{2-}$ was modeled in three positions, with a 57/37/6 occupancy ratio respectively. The cavities where the solvents are housed are larger than the volume of the solvent molecule, so in the three cavities the solvent presents occupational disorder with an occupation relationship as follows: 78/22, 35/32/17/15, and 52/25/23 respectively.

The molecular graphics were prepared using Ortep3, POV-RAY and GIMP.[70] Crystallographic data for the two crystal structures have been deposited with the Cambridge Crystallographic Data Centre, CCDC no. 2279289 and 2279290.† X-ray crystallographic data in the CIF format are available in the ESI.†

Conflicts of interest

There are no conflicts to declare.

Acknowledgements

We thank M. Sc. Eréndira García Rios, M. Sc. Lucero Mayra Ríos Ruiz, M. Sc. Lucía del Carmen Márquez Alonso, Dra. Beatriz Quiroz-García, Dra. Adriana Romo Pérez, Dra. Isabel Chávez Uribe and M. Sc. Elizabeth Huerta Salazar for technical assistance. We thank PAPIIT-UNAM 220023 and CONACYT PRONACES-160671 for financial support. M. K. S.-F. and A. O. V.-P. are grateful to CONAHCyT for scholarships 848759 and 868013. J. B. F. is grateful to DGTIC-UNAM for the use of the supercomputer Miztli.

References

1 M. Li, W. Zhu, F. Marken and T. D. James, Electrochemical sensing using boronic acids, *Chem. Commun.*, 2015, **51**, 14562–14573.
2 S. Yazdanpanah, M. Rabiee, M. Tahriri, M. Abdolrahim and L. Tayebi, Glycated hemoglobin-detection methods based on electrochemical biosensors, *TrAC, Trends Anal. Chem.*, 2015, **72**, 53–67.
3 J. Y. Wang, T. C. Chou, L. C. Chen and K. C. Ho, Using poly (3-aminophenylboronic acid) thin film with binding-induced ion flux blocking for amperometric detection of hemoglobin A1c, *Biosens. Bioelectron.*, 2014, **63**, 317–324.
4 J. I. Anzai, Recent progress in electrochemical biosensors based on phenylboronic acid and derivatives, *Mater. Sci. Eng., C*, 2016, **67**, 737–746.
5 H. Shahbazmohammadi, S. Sardari and E. Omidinia, An amperometric biosensor for specific detection of glycated hemoglobin based on recombinant engineered fructosyl peptide oxidase, *Int. J. Biol. Macromol.*, 2020, **142**, 855–865.
6 J. S. Hansen, M. Ficker, J. F. Petersen, J. B. Christensen and T. Hoeg-Jensen, Ortho-Substituted fluorescent aryl monoboronic acid displays physiological binding of D-glucose, *Tetrahedron Lett.*, 2013, **54**, 1849–1852.

7 A. Stubelius, S. Lee and A. Almutairi, The Chemistry of Boronic Acids in Nanomaterials for Drug Delivery, *Acc. Chem. Res.*, 2019, **52**, 3108–3119.
8 P. Keil, H. B. Mortensen and C. Christophersen, Fructosilvaline. A simple model of the N-terminal residue of human haemoglobin A1c, *Acta Chem. Scand., Ser. B*, 1985, **39**, 191–193.
9 S. Chawla and C. S. Pundir, An electrochemical biosensor for fructosyl valine for glycosylated hemoglobin detection based on core-shell magnetic bionanoparticles modified gold electrode, *Biosens. Bioelectron.*, 2011, **26**, 3438–3443.
10 C. Gerke, M. Buchholz, H. Müller, R. Meusinger, M. Grimmler and E. Metzmann, Direct glucosone-based synthesis and HILIC-ESI-MS/MS characterization of N-terminal fructosylated valine and valylhistidine for validation of enzymatic HbA1c assays in the diagnosis of diabetes mellitus, *Anal. Bioanal. Chem.*, 2019, **411**, 7967–7979.
11 S. Liu, J. Leng and T. C. Aquino, Development of Disposable Single-Use Biosensor for Fructosyl Valine and Glycated Hemoglobin A1c, *J. Sens. Technol.*, 2019, **09**, 45–53.
12 A. D. Troise, A. Fiore, G. Roviello, S. M. Monti and V. Fogliano, Simultaneous quantification of amino acids and Amadori products in foods through ion-pairing liquid chromatography-high-resolution mass spectrometry, *Amino Acids*, 2015, **47**, 111–124.
13 A. Sakaguchi, S. Ferri, W. Tsugawa and K. Sode, Novel fluorescent sensing system for α-fructosyl amino acids based on engineered fructosyl amino acid binding protein, *Biosens. Bioelectron.*, 2007, **22**, 1933–1938.
14 M. Hatada, S. Saito, S. Yonehara, W. Tsugawa, R. Asano, K. Ikebukuro and K. Sode, Development of glycated peptide enzyme sensor based flow injection analysis system for haemoglobin A1c monitoring using quasi-direct electron transfer type engineered fructosyl peptide oxidase, *Biosens. Bioelectron.*, 2021, **177**, 112984.
15 C. S. Pundir and S. Chawla, Determination of glycated hemoglobin with special emphasis on biosensing methods, *Anal. Biochem.*, 2014, **444**, 47–56.
16 Z. Zhan, Y. Li, Y. Zhao, H. Zhang, Z. Wang, B. Fu and W. J. Li, A Review of Electrochemical Sensors for the Detection of Glycated Hemoglobin, *Biosensors*, 2022, **12**, 1–23.
17 B. Wang and J. I. Anzai, Recent progress in electrochemical HbA1c sensors: A review, *Materials*, 2015, **8**, 1187–1203.
18 U. Jain, S. Gupta and N. Chauhan, Construction of an amperometric glycated hemoglobin biosensor based on Au–Pt bimetallic nanoparticles and poly (indole-5-carboxylic acid) modified Au electrode, *Int. J. Biol. Macromol.*, 2017, **105**, 549–555.
19 U. Jain, S. Gupta and N. Chauhan, Detection of glycated hemoglobin with voltammetric sensing amplified by 3D-structured nanocomposites, *Int. J. Biol. Macromol.*, 2017, **101**, 896–903.
20 S. Chawla and C. S. Pundir, An amperometric hemoglobin A1c biosensor based on immobilization of fructosyl amino acid oxidase onto zinc oxide nanoparticles-polypyrrole film, *Anal. Biochem.*, 2012, **430**, 156–162.
21 J. Y. Park, B. Y. Chang, H. Nam and S. M. Park, Selective electrochemical sensing of glycated hemoglobin (HbA1c) on thiophene-3-boronic acid self-assembled monolayer covered gold electrodes, *Anal. Chem.*, 2008, **80**, 8035–8044.
22 H. C. Chien and T. C. Chou, A Nonenzymatic Amperometric Method for Fructosyl-Valine Sensing Using Ferroceneboronic Acid, *Electroanalysis*, 2011, **23**, 402–408.
23 S. Liu, U. Wollenberger, M. Katterle and F. W. Scheller, Ferroceneboronic acid-based amperometric biosensor for glycated hemoglobin, *Sens. Actuators, B*, 2006, **113**, 623–629.
24 R. Rajkumar, A. Warsinke, H. Möhwald, F. W. Scheller and M. Katterle, Development of fructosyl valine binding polymers by covalent imprinting, *Biosens. Bioelectron.*, 2007, **22**, 3318–3325.
25 G. Springsteen and B. Wang, A detailed examination of boronic acid-diol complexation, *Tetrahedron*, 2002, **58**, 5291–5300.
26 J. Zamora-Moreno, M. K. Salomón-Flores, J. Valdes-García, C. Pinzón-Vanegas, D. Martínez-Otero, J. Barroso-Flores, R. Villamil-Ramos, M. A. Romero-Solano and A. Dorazco-González, Water-soluble fluorescent chemosensor for sorbitol based on a dicationic diboronic receptor. Crystal structure and spectroscopic studies, *RSC Adv.*, 2023, **13**, 32185–32198.
27 L. R. Ortega-Valdovinos, J. Valdes-García, I. J. Bazany-Rodríguez, J. C. Lugo-González, A. Dorazco-González and A. K. Yatsimirsky, Anion recognition by anthracene appended ortho-aminomethylphenylboronic acid: a new PET-based sensing mechanism, *New J. Chem.*, 2021, **45**, 15618–15628.
28 J. A. Peters, Interactions between boric acid derivatives and saccharides in aqueous media: Structures and stabilities of resulting esters, *Coord. Chem. Rev.*, 2014, **268**, 1–22.
29 Z. Guo, I. Shin and J. Yoon, Recognition and sensing of various species using boronic acid derivatives, *Chem. Commun.*, 2012, **48**, 5956–5967.
30 T. Pradhan, H. S. Jung, J. H. Jang, T. W. Kim, C. Kang and J. S. Kim, Chemical sensing of neurotransmitters, *Chem. Soc. Rev.*, 2014, **43**, 4684–4713.
31 C. W. Gray and T. A. Houston, Boronic acid receptors for α-hydroxycarboxylates: High affinity of Shinkai's glucose receptor for tartrate, *J. Org. Chem.*, 2002, **67**, 5426–5428.
32 J. Valdes-García, J. Zamora-Moreno, M. K. Salomón-Flores, D. Martínez-Otero, J. Barroso-Flores, A. K. Yatsimirsky, I. J. Bazany-Rodríguez and A. Dorazco-González, Fluorescence Sensing of Monosaccharides by Bis-boronic Acids Derived from Quinolinium Dicarboxamides: Structural and Spectroscopic Studies, *J. Org. Chem.*, 2023, **88**, 2174–2189.
33 Y. Kubo, F. Marken, K. Sakurai, J. Zhao and T. D. James, Exploiting the Reversible Covalent Bonding of Boronic Acids: Recognition, Sensing, and Assembly, *Acc. Chem. Res.*, 2013, **46**, 312–326.
34 W. L. A. Brooks, C. C. Deng and B. S. Sumerlin, Structure-Reactivity Relationships in Boronic Acid-Diol Complexation, *ACS Omega*, 2018, **3**, 17863–17870.

35 J. Yan, G. Springsteen, S. Deeter and B. Wang, The relationship among pKa, pH, and binding constants in the interactions between boronic acids and diols-it is not as simple as it appears, *Tetrahedron*, 2004, **60**, 11205–11209.
36 X. Zhang, G. Liu, Z. Ning and G. Xing, Boronic acid-based chemical sensors for saccharides, *Carbohydr. Res.*, 2017, **452**, 129–148.
37 A. Chaicham, S. Sahasithiwat, T. Tuntulani and B. Tomapatanaget, Highly effective discrimination of catecholamine derivatives via FRET-on/off processes induced by the intermolecular assembly with two fluorescence sensors, *Chem. Commun.*, 2013, **49**, 9287–9289.
38 A. M. Agafontsev, A. Ravi, T. A. Shumilova, A. S. Oshchepkov and E. A. Kataev, Molecular Receptors for Recognition and Sensing of Nucleotides, *Chem. – Eur. J.*, 2019, **25**, 2684–2694.
39 H. Otsuka, E. Uchimura, H. Koshino, T. Okano and K. Kataoka, Anomalous Binding Profile of Phenylboronic Acid with N-Acetylneuraminic Acid (Neu5Ac) in Aqueous Solution with Varying pH, *J. Am. Chem. Soc.*, 2010, **11**, 3493–3502.
40 C. R. Cooper and T. D. James, Selective D-glucosamine hydrochloride fluorescence signalling based on ammonium cation and diol recognition, *Chem. Commun.*, 1997, **15**, 1419–1420.
41 A. E. Hargrove, R. N. Reyes, I. Riddington, E. V. Anslyn and J. L. Sessler, Boronic acid porphyrin receptor for ginsenoside sensing, *Org. Lett.*, 2010, **12**, 4804–4807.
42 K. S. Ahn, J. H. Lee, J. M. Park, H. N. Choi and W. Y. Lee, Luminol chemiluminescence biosensor for glycated hemoglobin (HbA1c) in human blood samples, *Biosens. Bioelectron.*, 2016, **75**, 82–87.
43 X. Huang, Y. Han, J. Li, M. Tang and G. Qing, Sensitive and specific detection of saccharide species based on fluorescence: update from 2016, *Anal. Bioanal. Chem.*, 2023, **415**, 4061–4077.
44 B. Gyurcsik, T. Gajdab, L. Nagyb, K. Burger, A. Rockenbauer and L. Korecz, Proton, copper(II) and nickel(II) complexes of some amadori rearrangement products of D-glucose and amino acids, *Inorg. Chim. Acta*, 1993, **214**, 57–66.
45 Y. Zhou and J. Yoon, Recent progress in fluorescent and colorimetric chemosensors for detection of amino acids, *Chem. Soc. Rev.*, 2012, **41**, 52–67.
46 H. Aït-Haddou, S. L. Wiskur, V. M. Lynch and E. V. Anslyn, Achieving large color changes in response to the presence of amino acids: A molecular sensing ensemble with selectivity for aspartate, *J. Am. Chem. Soc.*, 2001, **123**, 11296–11297.
47 I. J. Bazany-Rodríguez, M. K. Salomón-Flores, J. M. Bautista-Renedo, N. González-Rivas and A. Dorazco-González, Chemosensing of Guanosine Triphosphate Based on a Fluorescent Dinuclear Zn(II)-Dipicolylamine Complex in Water, *Inorg. Chem.*, 2020, **59**, 7739–7751.
48 B. Watanabe, A. Ichiyanagi, K. Hirokawa, K. Gomi, T. Nakatsu and H. Kato, Synthesis and inhibitory activity of substrate-analog fructosyl peptide oxidase inhibitors, *Bioorg. Med. Chem. Lett.*, 2015, **25**, 3910–3913.
49 S. Gamsey, N. A. Baxter, Z. Sharrett, D. B. Cordes, M. M. Olmstead, R. A. Wessling and B. Singaram, The effect of boronic acid-positioning in an optical glucose-sensing ensemble, *Tetrahedron*, 2006, **62**, 6321–6331.
50 I. J. Bazany-Rodríguez, M. K. Salomón-Flores, A. O. Viviano-Posadas, M. A. García-Eleno, J. Barroso-Flores, D. Martínez-Otero and A. Dorazco-González, Chemosensing of neurotransmitters with selectivity and naked eye detection of L-DOPA based on fluorescent Zn(II)-terpyridine bearing boronic acid complexes, *Dalton Trans.*, 2021, **50**, 4255–4269.
51 R. Badugu, J. R. Lakowicz and C. D. Geddes, Boronic acid fluorescent sensors for monosaccharide signaling based on the 6-methoxyquinolinium heterocyclic nucleus: Progress toward noninvasive and continuous glucose monitoring, *Bioorg. Med. Chem.*, 2005, **13**, 113–119.
52 I. J. Bazany-Rodríguez, D. Martínez-Otero, J. Barroso-Flores, A. K. Yatsimirsky and A. Dorazco-González, Sensitive water-soluble fluorescent chemosensor for chloride based on a bisquinolinium pyridine-dicarboxamide compound, *Sens. Actuators, B*, 2015, **221**, 1348–1355.
53 W. F. Jager, T. S. Hammink, O. van den Berg and F. C. Grozema, Highly sensitive water-soluble fluorescent pH sensors based on the 7-amino-1-methylquinolinium chromophore., *J. Org. Chem.*, 2010, **75**, 2169–2178.
54 R. Hosseinzadeh, M. Mohadjerani, M. Pooryousef, A. Eslami and S. Emami, A new boronic acid fluorescent sensor based on fluorene for monosaccharides at physiological pH, *Spectrochim. Acta, Part A*, 2015, **144**, 53–60.
55 R. Badugu, J. R. Lakowicz and C. D. Geddes, Fluorescence sensors for monosaccharides based on the 6-methylquinolinium nucleus and boronic acid moiety: Potential application to ophthalmic diagnostics, *Talanta*, 2005, **65**, 762–768.
56 X. Chen, S. L. Chew, F. M. Kerton and N. Yan, Direct conversion of chitin into a N-containing furan derivative, *Green Chem.*, 2014, **16**, 2204–2212.
57 P. Barraud, M. Schubert and F. H. T. Allain, A strong ^{13}C chemical shift signature provides the coordination mode of histidines in zinc-binding proteins, *J. Biomol. NMR*, 2012, **53**, 93–101.
58 G. Fang, H. Wang, Z. Bian, J. Sun, A. Liu, H. Fang, B. Liu, Q. Yao and Z. Wu, Recent development of boronic acid-based fluorescent sensors, *RSC Adv.*, 2018, **8**, 29400–29427.
59 M. Yamamoto, M. Takeuchi and S. Shinkai, Molecular design of a PET-based chemosensor for uronic acids and sialic acids utilizing a cooperative action of boronic acid and metal chelate, *Tetrahedron*, 1998, **54**, 3125–3140.
60 J. Du, Z. Huang, X.-Q. Yu and L. Pu, Highly selective fluorescent recognition of histidine by a crown ether–terpyridine–Zn(II) sensor, *Chem. Commun.*, 2013, **49**, 5399–5401.
61 M. Takeuchi, M. Yamamoto and S. Shinkai, Fluorescent sensing of uronic acids based on a cooperative action of boronic acid and metal chelate, *Chem. Commun.*, 1997, **18**, 1731–1732.
62 M. K. Salomón-Flores, C. L. Hernández-Juárez, I. J. Bazany-Rodríguez, J. Barroso-Flores, D. Martínez-Otero, R. López-

Arteaga, J. Valdés-Martínez and A. Dorazco-González, Efficient fluorescent chemosensing of iodide based on a cationic meso-tetraarylporphyrin in pure water, *Sens. Actuators, B*, 2019, **281**, 462–470.

63 Q. Zhang, X. Tian, Z. Hu, C. Brommesson, J. Wu, H. Zhou, S. Li, J. Yang, Z. Sun, Y. Tian and K. Uvdal, A series of Zn (II) terpyridine complexes with enhanced two-photon-excited fluorescence for in vitro and in vivo bioimaging, *J. Mater. Chem. B*, 2015, **3**, 7213–7221.

64 G. Springsteen and B. Wang, Alizarin Red S. as a general optical reporter for studying the binding of boronic acids with carbohydrates, *Chem. Commun.*, 2001, 1608–1609.

65 M. J. Frisch, G. W. Trucks, H. B. Schlegel, G. E. Scuseria, M. A. Robb, J. R. Cheeseman, G. Scalmani, V. Barone, G. A. Petersson, H. Nakatsuji, X. Li, M. Caricato, A. V. Marenich, J. Bloino, B. G. Janesko, R. Gomperts, B. Mennucci, H. P. Hratchian, J. V. Ortiz, A. F. Izmaylov, J. L. Sonnenberg, D. Williams-Young, F. Ding, F. Lipparini, F. Egidi, J. Goings, B. Peng, A. Petrone, T. Henderson, D. Ranasinghe, V. G. Zakrzewski, J. Gao, N. Rega, G. Zheng, W. Liang, M. Hada, M. Ehara, K. Toyota, R. Fukuda, J. Hasegawa, M. Ishida, T. Nakajima, Y. Honda, O. Kitao, H. Nakai, T. Vreven, K. Throssell, J. A. Montgomery Jr., J. E. Peralta, F. Ogliaro, M. J. Bearpark, J. J. Heyd, E. N. Brothers, K. N. Kudin, V. N. Staroverov, T. A. Keith, R. Kobayashi, J. Normand, K. Raghavachari, A. P. Rendell, J. C. Burant, S. S. Iyengar, J. Tomasi, M. Cossi, J. M. Millam, M. Klene, C. Adamo, R. Cammi, J. W. Ochterski, R. L. Martin, K. Morokuma, O. Farkas, J. B. Foresman and D. J. Fox, *Gauss View 5.0*, Gaussian, Inc., Wallingford, USA, 2016.

66 *APEX 2 Softw. Suite*, Bruker AXS Inc., Madison, Wisconsin, USA, 2004.

67 G. M. Sheldrick, SHELXT – Integrated space-group and crystal-structure determination, *Acta Crystallogr., Sect. A: Found. Adv.*, 2015, **71**, 3–8.

68 C. B. Hübschle, G. M. Sheldrick and B. Dittrich, ShelXle: A Qt graphical user interface for SHELXL, *J. Appl. Crystallogr.*, 2011, **44**, 1281–1284.

69 G. M. Sheldrick, *SHELXL-97, Progr. Cryst. Struct. Refinement*, Univ. Göttingen.

70 L. J. Farrugia, *Ortep-3 for Windows, Ortep-3 Wind*, **https://www.chem.gla.ac.uk/~louis/software/ortep/**.